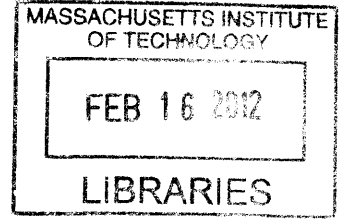# Flexible Dynamics of Floating Wind Turbines

by

Thomas Luypaert

Ingénieur de l'École Centrale Paris, 2009

Submitted to the Department of Mechanical Engineering
in partial fulfillment of the requirements for the degree of

Master of Science in Mechanical Engineering
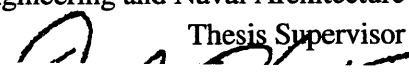at the
Massachusetts Institute of Technology

February 2012

Author ....
Department of Mechanical Engineering
September 26, 2011

Certified by...
Paul D. Sclavounos
Professor of Mechanical Engineering and Naval Architecture
Thesis Supervisor

Accepted by..
David E. Hardt
Professor of Mechanical Engineering
Chairman, Department Committee on Graduate Students

Abstract

This work presents Tower Flex, a structural dynamics model for a coupled analysis of offshore floating wind turbines consisting of a tower, a floating platform and a mooring system. In this multi-body, linear frequency-domain model, the tower is represented as a series of uniform Timoshenko beams connected to each other. The deflections of the tower are solved analytically in each beam while the mass, damping and stiffness coming from the rotor, the floating platform and the mooring lines are taken into account *via* generalized boundary conditions.

Tower Flex is used for the evaluation of a 3MW offshore floating wind turbine mounted on a Tension Leg Platform (TLP). Natural frequencies, motion responses and fatigue damage are analyzed to illustrate the features of Tower Flex and assess the performance of the proposed design.

Acknowledgements

Table of Contents

Table of Symbols and Abbreviations

Latin symbols

Symbol	Unit	Description
A	[m]	Incident wave amplitude
	[m^2]	Shear area
A_{ij}	[kg, kg.m, kg.m^2]	(i,j) component of the added mass matrix
A_g	[m^2]	Geometric area
A_w	[m^2]	Water plane area
B_{ij}^{AERO}	[kg/s, kg.m/s, kg.m^2/s]	(i,j) component of the aerodynamic damping matrix
B_{ij}^{HYDRO}	[kg/s, kg.m/s, kg.m^2/s]	(i,j) component of the hydrodynamic damping matrix
C	[MPa^m]	Constant in fatigue law
$\{C\}$	[-]	Mode shape vector
C_{ij}^{HI}	[kg/s^2, kg.m/s^2, kg.m^2/s^2]	(i,j) component of the hydrostatic restoring matrix
C_{ij}^{LINES}	[kg/s^2, kg.m/s^2, kg.m^2/s^2]	(i,j) component of the linear restoring matrix from the mooring lines
D	[-]	Fatigue damage
E	[N/m^2]	Young's modulus
f	[Hz]	Frequency
F_j^{AERO}	[N, N.m]	j-th component of the wind load on the buoy
F_j^{HYDRO}	[N/m, N.m/m]	j-th component of the wave load on the buoy for a unit wave amplitude
$\{F\}$	[-]	Force vector
g	[m/s^2]	Gravitational acceleration constant
G	[N/m^2]	Shear modulus
H_s	[m]	Significant wave height
H_{σ_i}	[MPa/N, MPa/N.m]	Stress transfer function from unit load in direction i
I	[m^4]	Polar moment of inertia of the cross-section
J	[kg.m]	Mass moment inertia of the cross-section
J_{rot}	[kg.m^2]	Mass moment of inertia of the rotor
k	[-]	Shear parameter
	[-]	Shape parameter of the Weibull

		distribution
L	[m]	Beam length
m	[kg/m]	Cross-sectional mass
	[-]	Fatigue exponent
M	[N.m]	Bending moment
M_{ii}	[kg, kg.m, kg.m^2]	(i,j) component of the total mass matrix
N	[-]	Number of beam segments
		Number of cycles to failure
n_0^+	[Hz]	Expected frequency of response
n_p^+	[Hz]	Mean number of maxima of the response
P	[N]	Axial load on the beam
q	[-]	Distribution of stress peaks
r	[m]	Buoy radius
	[m]	Radius of gyration
	[-]	Irregularity factor
R	[m]	Cross-sectional radius
S_{wave}	[m^2/Hz, m^2/rad/s]	Wave spectrum
$S_{i\,wind}$	[N^2/Hz, N^2.m^2/Hz]	Spectral density of the wind load in direction i
$S_{\sigma_{wave}}$	[MPa^2/Hz, MPa^2/rad/s]	Spectral density of the stress due to wave loads
$S_{\sigma_{wind}}$	[MPa^2/Hz]	Spectral density of the stress due to wind loads
$[S]$	[-]	Force matrix
t	[m]	Cross-sectional thickness
T	[s]	Fatigue lifetime
T_p	[s]	Mean spectral period
U	[m/s]	Wind speed
V	[N]	Shear force
ϑ	[m^3]	Immersed volume
w	[m]	Displacement of the middle line of the beam
X_j	[m, -]	j-th component of the tower displacement
$\{X\}$	[-]	Displacement vector
z_B	[m]	Vertical location of the center of buoyancy from the free surface
z_G	[m]	Vertical location of the center of gravity from the free surface
$[Z]$	[-]	Displacement matrix

Greek symbols

Symbol	Unit	Description
$\dot{\alpha}$	[rad/s]	Rotor angular velocity
γ	[rad]	Shear angle
	[-]	Incomplete gamma function
Γ	[-]	Gamma function
ν	[-]	Poisson's ratio
ω	[rad/s]	Angular frequency
ρ	[kg/m^3]	Density
σ	[m]	Root mean square
	[MPa]	Stress level
θ	[rad]	Rotation of the cross-section

Abbreviations

DLC	Design Load Case
DNV	Det Norske Veritas
DOF	Degree Of Freedom
FA	Fore-Aft
ITTC	International Towing Tank Conference
PSD	Power Spectral Density
RAO	Response Amplitude Operator
RMS	Root Mean Square
RPM	Rotations Per Minute
STS	Side-To-Side
TLP	Tension Leg Platform
WAMIT	Wave Analysis at MIT

List of figures

List of tables

Introduction

Over the past decade, rising energy costs together with concerns about energy security and the effect of anthropogenic greenhouse gases on the climate have pushed towards the adoption of renewable sources of energy (hydro, wind, solar, biomass). Among these, wind has been the leading source in terms of added capacity, sometimes even topping conventional power sources like natural gas in the European Union in 2008 and 2009 [20].

Today, almost all of the world's total 200GW wind capacity is still located onshore [21]. However, stronger and steadier winds offshore offer a vast and yet largely untapped resource that could be harnessed to supply coastal population centers with renewable power.

As of 2010, all operational offshore wind farms are located in the European Union and total 3GW of capacity [20]. All of them feature wind turbines mounted on various types of fixed structures (e.g. monopiles) lying on the seabed. While this solution is attractive in shallow water depths, it becomes too expensive to reach water depths above 50m. This currently prevents offshore wind farms to be installed in certain coastal areas where water depth is high, like the Mediterranean Sea [22]. It also constitutes a major hurdle if we are to address the repeated "Not In My Backyard" concerns by reaching the 20-30 km distance where wind turbines are no longer visible from the shore.

To overcome the water depth constraint, floating wind turbines have emerged as a promising solution. Various concepts have been proposed, most of which are inspired by technologies developed by the offshore oil & gas industry. The concepts for the floating platform can roughly be divided into three categories: 1. Spar buoys [11], 2. Semi-submersibles [12] and 3. Tension Leg Platforms (TLPs) [6,7].

Comparing the respective merits of these designs is beyond the scope of this thesis and has already been very well documented [8]. Instead, we shall discuss the development of Tower Flex, a linear, frequency-domain structural dynamics code for floating wind turbines, and its application to the evaluation of a modified 3MW TLP concept designed at MIT. Compared to previous work [6,7], Tower Flex accounts for the deformations of the tower which allows for a rigorous assessment of the TLP.

Chapter 1 provides a general description of the proposed TLP design while Chapter 2 discusses the theory and implementation of Tower Flex. Chapters 3 and 4 present the results for the natural frequencies and motion responses in order to assess the performance of the TLP design and validate Tower Flex. Finally, Chapter 5 is devoted to the fatigue analysis in the frequency domain.

1 Description of the TLP design

1. Blades
2. Nacelle + Hub
3. Tower
4. Transition piece
5. Buoy
6. Braces
7. Mooring lines
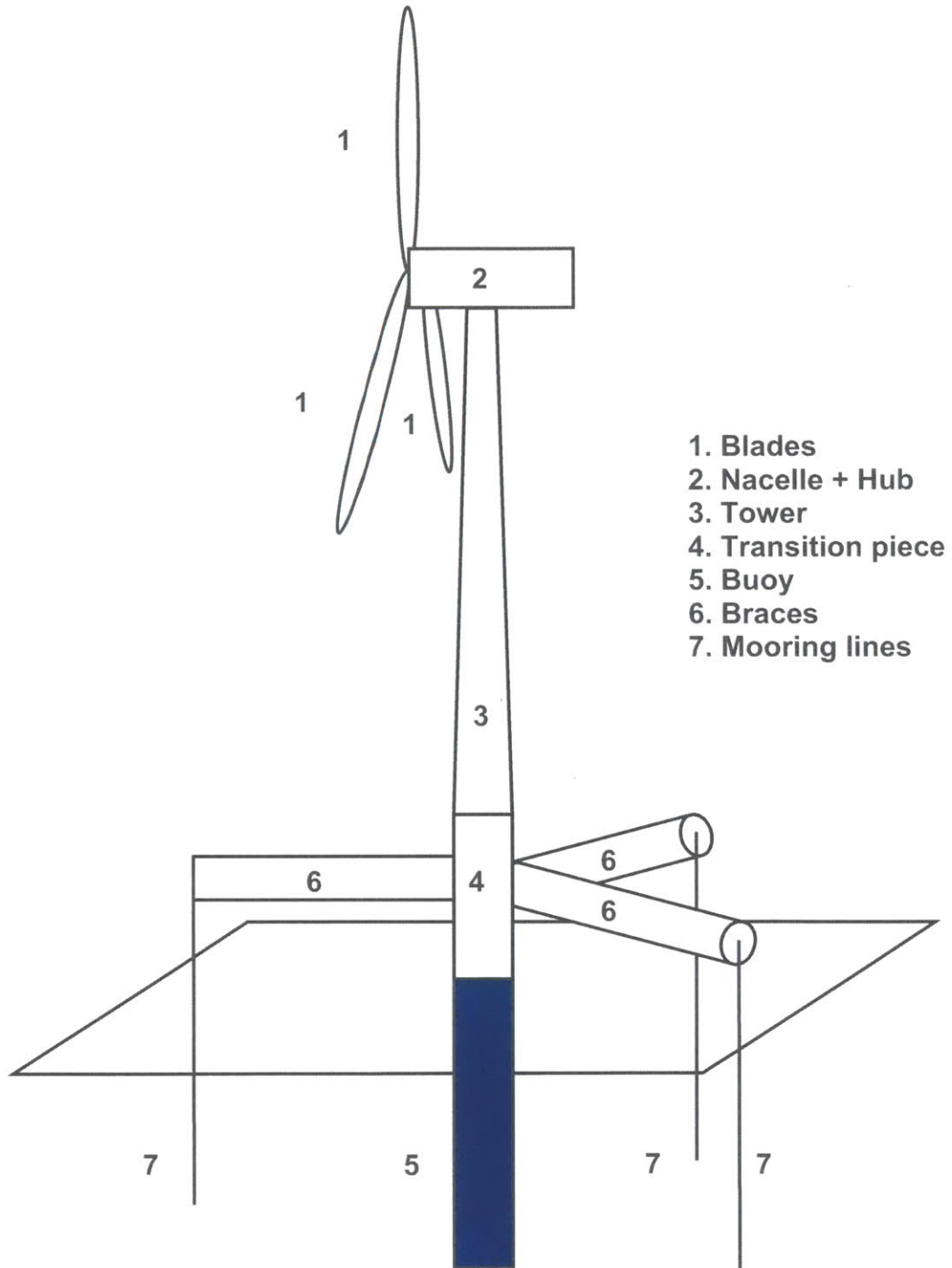
Figure 1: Side view of the TLP

1.1 Specifications of the TLP design

The TLP design is illustrated in Figure 1. In this structure, a conventional three-bladed horizontal axis wind turbine (comprising the tower, the nacelle, the hub and the blades) is connected to a cylindrical buoy by a transition piece (TP). The transition piece supports three horizontal braces that are equally spaced around the tower. The structure is anchored to the seabed (not represented here) by vertical mooring lines attached to the tip of the braces. Unlike previous designs [6,7], the structure has no concrete or water ballasts. The mooring lines are therefore pre-tensioned to compensate for the excess buoyancy and ensure static vertical equilibrium. The main specifications of the system are detailed in Table 1 below.

Sea State	Water depth [m]	100.0
	Significant wave height Hs [m]	10.0
	Mean spectral period [s]	13.6

Wind turbine (without TP)	Rated power [MW]	3.0
	Cut-in wind speed [m/s]	3.0
	Cut-out wind speed [m/s]	25.0
	Rated wind speed [m/s]	11.0
	Hub height [m]	80.0
	Tower diameter [m]	[2.8-4.2]
	Total mass [tons]	393

Transition piece (without braces)	Diameter [m]	4.2
	Height [m]	25
	Steel thickness [mm]	50
	Steel mass [tons]	131
	Center of mass [m]	12.5
Braces	Number of braces	3
	Diameter [m]	5
	Height above sea level [m]	17.5
	Length [m]	10
	Steel thickness [mm]	50
	Steel mass (each) [tons]	62
Transition piece (total)	Steel mass [tons]	317
	Center of mass [m]	15.4

Mooring lines	Mooring system angle [deg]	90
	Number of lines per brace	2
	EA per line [N]	4.8E9
	E [Pa]	2.2E11
	Diameter per line [cm]	16.7
	Pretension per line [tons]	160

Buoy	Diameter [m]	4.9
	Draft [m]	25
	Center of mass [m]	-12.5
	Center of buoyancy [m]	-12.5
	Displacement [tons]	1,975
	Steel mass [tons]	256
	Steel Thickness [mm]	36
	Number of ring stiffeners	6

Complete structure	Total mass [tons]	966
	Total center of mass [m]	32.8
	Total center of buoyancy [m]	-12.5
	Static surge offset [m]	4.96
	Static pitch offset [deg]	0.13
	Line 1 Static tension [tons]	112
	Line 2 Static tension [tons]	255
	Line 3 Static tension [tons]	112

Table 1: Static specifications of the 3MW TLP

In addition to the TLP specifications presented above, we had at our disposal the thrust and RPM curves of the 3MW wind turbine over the range of operating wind speeds.

1.2 Description of the rigid-body motion

Before investigating the complete flexible dynamics of the floating wind turbine, we shall begin with the description of its rigid-body motion to introduce important definitions and concepts.

Given a particular wind speed and the thrust, a static mean thrust is applied to the TLP, which defines a mean offset position. Following the conventions of naval architecture [5], the three-dimensional motion of the structure is then described in an earth-fixed frame

centered at the TLP's mean offset position on the free surface. Figure 2 illustrates this reference frame as well as the six different degrees of freedom listed in Table 2.

Index	Degree of freedom (DOF)
1	Surge
2	Sway
3	Heave
4	Roll
5	Pitch
6	Yaw

Table 2: Degrees of freedom of the rigid TLP

The rigid body motion of the floating wind turbine can be analyzed by writing down Newton's law about the origin at the free surface for each of the six modes of motion

$$(\mathbf{M} + \mathbf{A})\ddot{\mathbf{x}} + \mathbf{B}\dot{\mathbf{x}} + \mathbf{C}\mathbf{x} = \mathbf{f}(t) \tag{1.1}$$

Where $\mathbf{A}$ is the 6x6 added mass matrix of the buoy, $\mathbf{M}$ is the 6x6 mass matrix, $\mathbf{B}$ is the 6x6 linear damping matrix, $\mathbf{C}$ is the 6x6 restoring matrix, $\mathbf{x}$ is the 6x1 vector of the floating wind turbine displacement from the origin and is the 6x1 vector of exciting aero- and hydrodynamic forces.

In order to evaluate the performance of the proposed design in random sea and wind conditions, a linear frequency-domain analysis is performed. The exciting forces and moments due to a plane progressive wave upon a floating wind turbine located at the origin of the coordinate system will be assumed to be of the form

$$f_j^{\text{HYDRO}}(t) = \text{Re}\left\{ F_j^{\text{HYDRO}}(\omega)e^{i\omega t} \right\}, \text{ j=1...6} \tag{1.2}$$

Similarly, the exciting forces and moments due to the wind will be assumed to be

$$f_j^{\text{AERO}}(t) = \text{Re}\left\{ F_j^{\text{AERO}}(\omega)e^{i\omega t} \right\}, \text{ j=1...6} \tag{1.3}$$

The response to such excitation, by virtue of linearity, will be of the form

$$x_j(t) = \text{Re}\left\{ X_j(\omega)e^{i\omega t} \right\}, \text{ j=1...6} \tag{1.4}$$

Where both $F_j(\omega)$ and $X_j(\omega)$ are complex quantities.[*]

---

[*] Since this work deals with both wind and wave excitations, we shall use X and F for the displacements and forces instead of the traditional Ξ and X used in hydrodynamics.
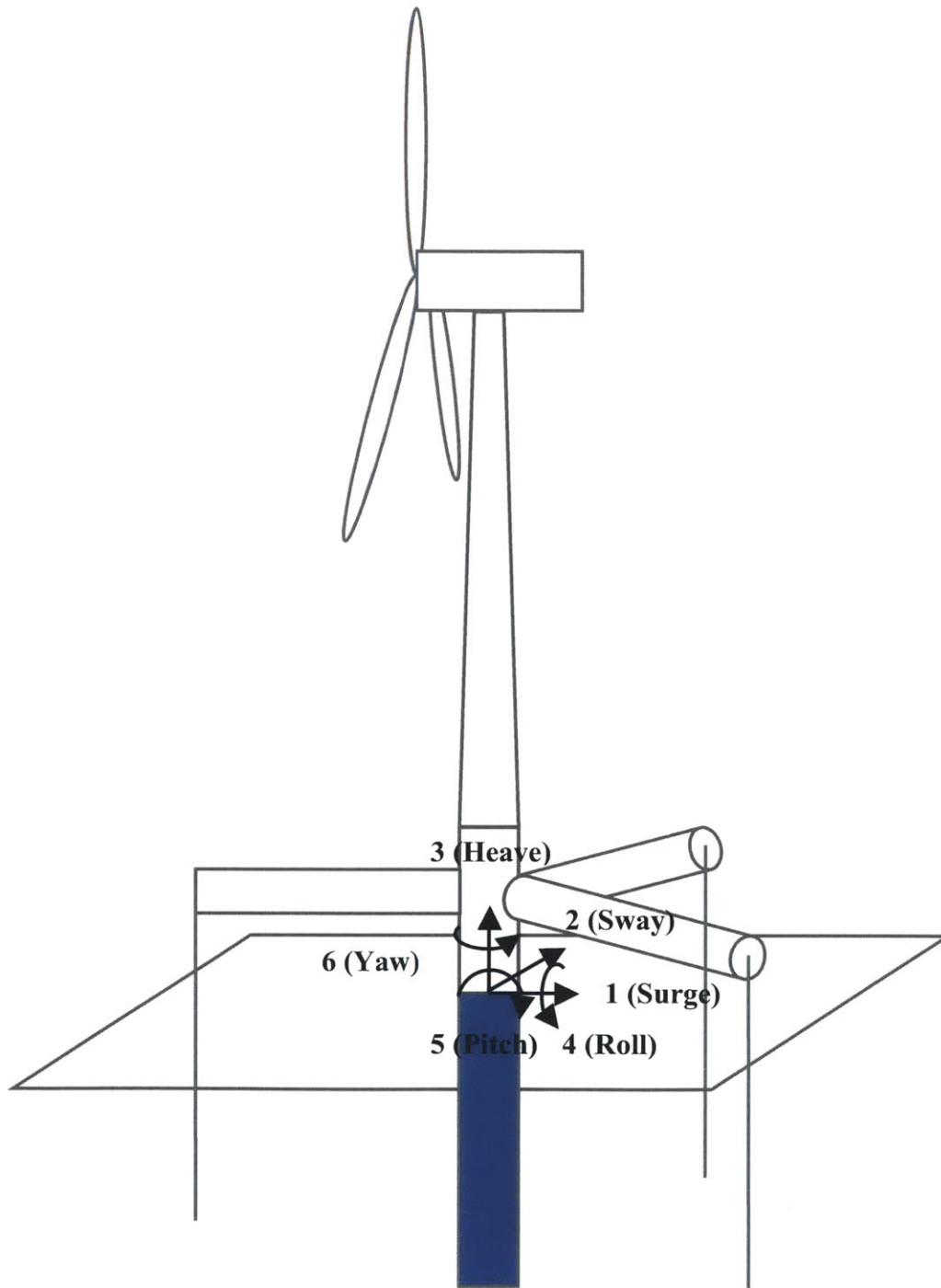
Figure 2: Definition of the global reference frame and coordinate system

1.2.1 RAOs

The main seakeeping quantity from a linear analysis of a floating body is the Response Amplitude Operator (RAO), which is defined as follows

$$RAO_j(\omega) = \frac{X_j(\omega)}{A/r^n}, \text{j=1}...6 \tag{1.5}$$

Where A is the incident wave amplitude, r is the radius of the buoy, and $n=0$ for j=1...3 and $n=1$ for j=4...6

The RAOs are found by solving the rigid-body equations of motion for the system in the frequency-domain

$$[-\omega^2(A_{ij}(\omega) + M_{ij}) + i\omega B_{ij}(\omega) + C_{ij}]X_j(\omega) = F_i^{\text{HYDRO}}(\omega) \text{ i, j=1..6} \tag{1.6}$$

1.2.2 Calculation of coefficients and excitations

We briefly discuss here the origin of the added-mass, damping and restoring mechanisms acting on the TLP. The actual values used in the modeling of the TLP can be found in paragraph 2.5

The linear restoring matrix C_{ij} is made of two components

$$C_{ij} = C_{ij}^{\text{HI}} + C_{ij}^{\text{LINES}} \tag{1.7}$$

where C_{ij}^{HI} is the hydrostatic and inertial restoring component and C_{ij}^{LINES} is the restoring component due to the mooring system.

The hydrostatic and inertial restoring coefficients are given by

$$\begin{aligned} C_{33}^{\text{HI}} &= \rho g A_w \\ C_{44}^{\text{HI}} &= C_{55}^{\text{HI}} = \rho \vartheta g z_B - M g z_G + \rho g \iint\limits_{A_w} x^2 \, dA \end{aligned} \tag{1.8}$$

Where A_w is the water plane area, ϑ the immersed volume, z_B and z_G the vertical location of the center of buoyancy and gravity respectively.

17

The linear C_{ij}^{LINES} matrix is evaluated by the in-house code LINES at the offset position under a mean wind thrust.

The linear damping matrix is also made of two components

$$B_{ij}(\omega) = B_{ij}^{\text{HYDRO}}(\omega) + B_{ij}^{\text{AERO}} \tag{1.9}$$

where $B_{ij}^{\text{HYDRO}}(\omega)$ is the frequency-dependent hydrodynamic wave damping calculated by WAMIT© and B_{ij}^{AERO} is the aerodynamic damping exerted on the rotor. Hydrodynamic viscous effects and the tower drag are neglected in the present work.

Finally the linear, added mass matrix $A_{ij}(\omega)$ is also calculated using WAMIT©.

1.3 Design flowchart
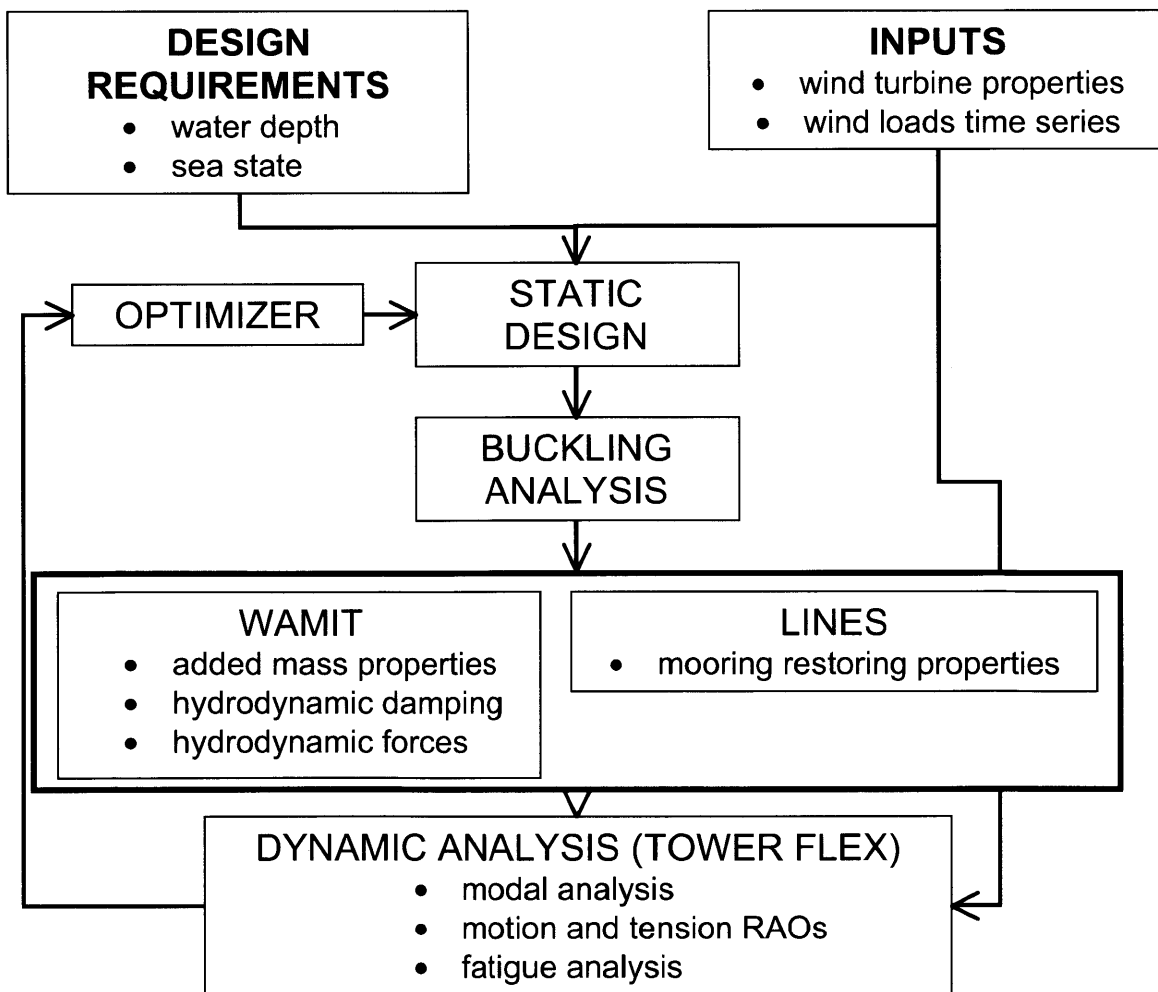
Figure 3: TLP Design flowchart

2 Structural dynamics in Tower Flex

2.1 Motivation

The main objective of this work is to model and understand the structural dynamics of the proposed TLP design. Key dynamic outputs include natural frequencies, motion and tension RAOs as well as fatigue loads. Building on previous work [6,7] carried out at MIT and based on rigid body dynamics, we shall now model the tower and the braces as flexible.

For the sake of accuracy and control over different outputs, we have adapted and extended an analytical model of a Timoshenko beam proposed by Arboleda [1]. This original model accounts for:

- bending and shear deformations along the beam (Timoshenko model)
- static axial loads due to gravity
- rotational inertia of the segments
- generalized boundary conditions with translational/rotational inertia and stiffness

We have extended this model to account for the specific features of the TLP design:

- a non-uniform tower geometry
- restoring effects from hydrostatics and the mooring lines
- hydrodynamic and aerodynamic damping
- hydrodynamic added mass
- three-dimensional effects

The resulting model is Tower Flex, a multi-body, frequency-domain structural dynamics code for a coupled analysis of floating wind turbines. In this model, the tower is modeled as a series of uniform Timoshenko beams connected to each other. The deflections of the tower are solved for analytically in each beam while the mass, damping and stiffness coming from the rotor, the floating platform and the mooring lines are taken into account *via* generalized boundary conditions. Tower Flex is described in great detail in the rest of this chapter. First, the original two-dimensional model and its extensions (2D Tower Flex) are introduced; then the three-dimensional model comprising the braces (3D Tower Flex) is presented; finally, the last section discusses the practical modeling of the TLP in Tower Flex.

2.2 2D Tower Flex

This section discusses the theoretical basis and the numerical implementation of the planar Timoshenko beam model proposed by Arboleda et al [1].

2.2.1 The Timoshenko beam model

Contrary to a classical Euler-Bernoulli beam, a Timoshenko beam is described by two independent geometric parameters as illustrated in Figure 4.
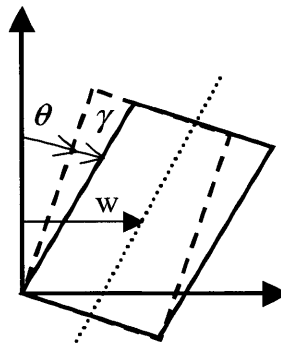
Figure 4: Description of the geometric parameters of a Timoshenko beam

w is the displacement of the middle line measured from its initial position

θ is the angle between the initial middle line and the line perpendicular to the face, representing the rotation due to bending

γ is the angle between the deflected middle line and the perpendicular to the face, representing the effect of shear. γ is related to the slope of the middle line w' by

$$\gamma = w' - \theta \qquad (2.1)$$

2.2.2 Equations of motion

The sketch of a differential Timoshenko beam element of with uniform linear mass m and rotational inertia J is represented in Figure 5.
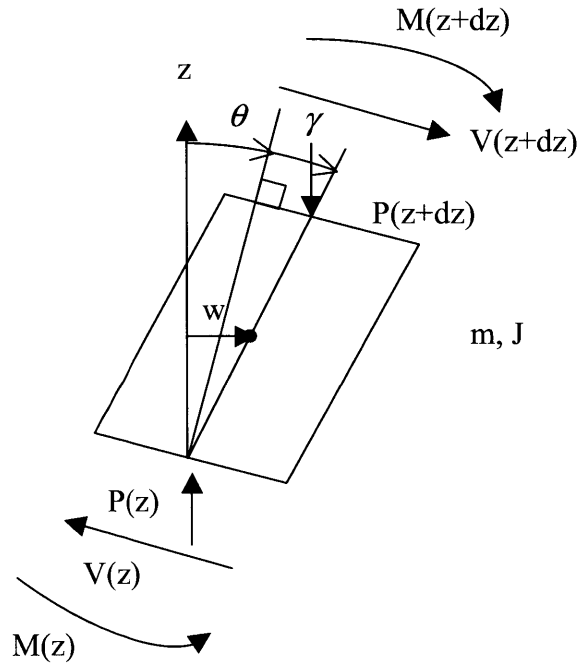
Figure 5: Differential Timoshenko beam element

The equations of motion can be derived by applying the linear and angular momentum principles to the center of gravity of the element. Assuming small displacements and keeping leading-order terms, we obtain

$$m\frac{\partial^2 w}{\partial t^2} = \frac{\partial V}{\partial z} \tag{2.2}$$

for the transverse equilibrium and

$$J\frac{\partial^2 \theta}{\partial t^2} = \frac{\partial M}{\partial z} + V + P\frac{\partial w}{\partial z} \tag{2.3}$$

for the rotational equilibrium.

These equations need to be combined with constitutive relationships for shear and bending.

Shear force equation

The compressive load P on a bended section adds to the shear, and this equivalent shear is related to the shear angle

$$V + P\theta = GA\gamma = GA\left(\frac{\partial w}{\partial z} - \theta\right) \qquad (2.4)$$

In this equation, A is the shear area of the section, which is proportional to the gross (geometric) area of the section according to

$$A = kA_g \qquad (2.5)$$

k is a parameter that depends on the geometry of the cross section and on the Poisson's ratio of the material v.

Bending moment equation

The bending moment on a section is proportional to the curvature of the middle line

$$M = EI\frac{\partial \theta}{\partial z} \qquad (2.6)$$

Substituting the constitutive relationships (2.5) and (2.6) into the equations of motion (2.2) and (2.3) yields

$$m\frac{\partial^2 w}{\partial t^2} = GA\frac{\partial^2 w}{\partial z^2} - (GA + P)\frac{\partial \theta}{\partial z}$$

$$J\frac{\partial^2 \theta(z,t)}{\partial t^2} = EI\frac{\partial^2 \theta}{\partial z^2} + (GA + P)\left(\frac{\partial w}{\partial z} - \theta\right)$$

Writing $w(z,t) = \Re\left[W(z)e^{i\omega t}\right]$ and $\theta(z,t) = \Re\left[\Theta(z)e^{i\omega t}\right]$, the general formulation of the frequency domain problem for a beam segment with uniform properties is

$$-m\omega^2 W(z) - GA\frac{d^2W}{dz^2} + (GA + P)\frac{d\Theta}{dz} = 0 \qquad (2.7)$$

$$EI\frac{d^2\Theta}{dz^2} - (GA + P - J\omega^2)\Theta + (GA + P)\frac{dW}{dz} = 0 \qquad (2.8)$$

These equations are the same as the ones given p 1061 in [1].

22

Dimensionless equations

Following Arboleda et al, equations (2.7) and (2.8) are divided by *GA* and *EI / L* respectively. In dimensionless form, the frequency-domain problem for a beam with uniform properties and axial loading P becomes

$$-b^2 s^2 \bar{W} - \frac{d^2 \bar{W}}{d\bar{z}^2} + (1 + F^2 s^2) \frac{d\Theta}{d\bar{z}} = 0 \tag{2.9}$$

$$s^2 \frac{d^2 \Theta}{d\bar{z}^2} - (1 + F^2 s^2 - b^2 s^2 R^2)\Theta + (1 + F^2 s^2) \frac{d\bar{W}}{d\bar{z}} = 0 \tag{2.10}$$

The parameters appearing in equations (2.9) and (2.10) are presented in Table 3 below. It should be noted that the mass moment of inertia *J* of a cross-section about its centroid is related to its polar moment of inertia *I* by $J = \rho I$. Using the radius of gyration, $J = \rho I = \rho A_g (I / A_g) = \bar{m} r^2$

Parameter	Description
$\bar{z} = z / L$	Dimensionless length
$\bar{W} = W / L$	Dimensionless deflection
$b^2 = \dfrac{m\omega^2}{EI / L^4}$	Frequency parameter
$s^2 = \dfrac{EI / L^2}{GA}$	Bending-to-shear stiffness parameter
$F^2 = \dfrac{P}{EI / L^2}$	Axial load parameter
$R^2 = \dfrac{r^2}{L^2}$, where $r^2 = I / A_g$	Slenderness parameter

Table 3: Dimensionless parameters in Tower Flex

Decoupling

Equations (2.9) and (2.10) are two coupled second-order ordinary differential equations (ODEs) that can be uncoupled as follows

Differentiate (2.9) with respect to $\bar{z}$

$$-b^2 s^2 \frac{d\bar{W}}{d\bar{z}} - \frac{d^3 \bar{W}}{d\bar{z}^3} + (1 + F^2 s^2) \frac{d^2 \Theta}{d\bar{z}^2} = 0 \tag{2.11}$$

From (2.10) we obtain

$$\frac{d\overline{W}}{d\overline{z}} = \left(1 - \frac{b^2 s^2 R^2}{1 + F^2 s^2}\right)\Theta - \frac{s^2}{1 + F^2 s^2}\frac{d^2\Theta}{d\overline{z}^2} \tag{2.12}$$

Which we can then differentiate twice with respect to $\overline{z}$

$$\frac{d^3\overline{W}}{d\overline{z}^3} = \left(1 - \frac{b^2 s^2 R^2}{1 + F^2 s^2}\right)\frac{d^2\Theta}{d\overline{z}^2} - \frac{s^2}{1 + F^2 s^2}\frac{d^4\Theta}{d\overline{z}^4} \tag{2.13}$$

Plug back this result into (2.11) and rearrange the terms

$$\frac{s^2}{1 + F^2 s^2}\frac{d^4\Theta}{d\overline{z}^4} + \left(\frac{b^2 s^4}{1 + F^2 s^2} - 1 + \frac{b^2 s^2 R^2}{1 + F^2 s^2} + 1 + F^2 s^2\right)\frac{d^2\Theta}{d\overline{z}^2} + \left(\frac{b^4 s^4 R^2}{1 + F^2 s^2} - b^2 s^2\right)\Theta = 0 \tag{2.14}$$

Finally multiply by $\dfrac{1 + F^2 s^2}{s^2}$ to obtain

$$\frac{d^4\Theta}{d\overline{z}^4} + \left(b^2 s^2 + b^2 R^2 + F^2 + F^4 s^2\right)\frac{d^2\Theta}{d\overline{z}^2} + \left(b^4 R^2 s^2 - b^2 - b^2 F^2 s^2\right)\Theta = 0 \tag{2.15}$$

An identical equation can similarly be obtained for $\overline{W}$

Solution

Equation (2.15) can be rewritten as

$$\frac{d^4\Theta}{d\overline{z}^4} + 2\Omega\frac{d^2\Theta}{d\overline{z}^2} + \varepsilon\Theta = 0 \tag{2.16}$$

with $\Omega = (b^2 s^2 + b^2 R^2 + F^2 + F^4 s^2)/2$ and $\varepsilon = b^4 R^2 s^2 - b^2 - b^2 F^2 s^2$

We look for the solutions of the characteristic equation

$$m^4 + 2\Omega m^2 + \varepsilon = 0 \tag{2.17}$$

At low frequencies (the cases that are relevant to us) $\Omega^2 > \varepsilon$ so that the discriminant $m^2 = -\Omega \pm \sqrt{\Omega^2 - \varepsilon}$ is real.

Case a) $\varepsilon < 0$

$$m = \pm i\beta, \pm \alpha$$
$$\alpha = \sqrt{-\Omega + \sqrt{\Omega^2 - \varepsilon}}$$
$$\beta = \sqrt{\Omega + \sqrt{\Omega^2 - \varepsilon}}$$

The solution for the deflection can therefore be written as a linear combination of trigonometric and hyperbolic functions

$$\overline{W} = C_1 \sin \beta \overline{z} + C_2 \cos \beta \overline{z} + C_3 \sinh \alpha \overline{z} + C_4 \cosh \alpha \overline{z} \qquad (2.18)$$

Similarly, the solution for the rotation can be written as

$$\Theta = C'_1 \sin \beta \overline{z} + C'_2 \cos \beta \overline{z} + C'_3 \sinh \beta \overline{z} + C'_4 \cosh \beta \overline{z} \qquad (2.19)$$

However the deflection W and the rotation Θ are *not* independent so there are *compatibility* conditions between the set of 4 coefficients $\{C\}$ and $\{C'\}$, where the shift in indices is actually a consequence of the relationship between W' and Θ

$$\begin{cases} C'_1 = -\lambda C_2 \\ C'_2 = \lambda C_1 \\ C'_3 = \delta C_4 \\ C'_4 = \delta C_3 \end{cases} \qquad (2.20)$$

with

$$\lambda = \frac{\beta^2 - b^2 s^2}{\beta(F^2 s^2 + 1)} \qquad (2.21)$$

and

$$\delta = \frac{\alpha^2 + b^2 s^2}{\alpha(F^2 s^2 + 1)} \qquad (2.22)$$

Case b) $0 < \varepsilon < \Omega^2$

$$m = \pm i\beta, \pm i\alpha$$
$$\alpha = \sqrt{\Omega - \sqrt{\Omega^2 - \varepsilon}} \quad \text{(new definition)}$$
$$\beta = \sqrt{\Omega + \sqrt{\Omega^2 - \varepsilon}} \quad \text{(unchanged)}$$

In this case, the solution is a linear combination of trigonometric functions only

$$\overline{W} = C_1 \sin\beta\overline{z} + C_2 \cos\beta\overline{z} + C_3 \sin\alpha\overline{z} + C_4 \cos\alpha\overline{z} \qquad (2.23)$$

Similarly, the solution for the rotation angle can be written as

$$\Theta = C'_1 \sin\beta\overline{z} + C'_2 \cos\beta\overline{z} + C'_3 \sin\alpha\overline{z} + C'_4 \cos\alpha\overline{z} \qquad (2.24)$$

The corresponding *compatibility* relations become (notice the change in C'_3)

$$\begin{cases} C'_1 = -\lambda C_2 \\ C'_2 = \lambda C_1 \\ C'_3 = -\delta C_4 \\ C'_4 = \delta C_3 \end{cases} \qquad (2.25)$$

with

$$\lambda = \frac{\beta^2 - b^2 s^2}{\beta(F^2 s^2 + 1)} \quad \text{(same definition)} \qquad (2.26)$$

and

$$\delta = \frac{\alpha^2 - b^2 s^2}{\alpha(F^2 s^2 + 1)} \quad \text{(new definition)} \qquad (2.27)$$

2.2.3 Boundary conditions and model outputs

Overall the 2D bending problem has only four unknowns represented by the 4x1 vector

$$\{C\} = \begin{pmatrix} C_1 \\ C_2 \\ C_3 \\ C_4 \end{pmatrix} \qquad (2.28)$$

Now we can relate $\{C\}$ to the *known* boundary conditions, either displacements or forces.

The dimensionless displacements and rotations at the boundaries are represented by the 4x1 vector

$$\{X\} = \begin{pmatrix} \bar{W}_0 \\ \Theta_0 \\ \bar{W}_1 \\ \Theta_1 \end{pmatrix} \tag{2.29}$$

They are related to $\{C\}$ by the matrix relationship

$$\{X\} = [Z]\{C\} \tag{2.30}$$

where $[Z]$ and is the 4x4 matrix presented p.1066 of [1].with $\rho = 1$ (meaning that the connections are perfectly rigid). $[Z]$ can be easily obtained by plugging $\bar{z} = 0$ and $\bar{z} = 1$ into (2.18) and (2.19), and making use of the compatibility relations (2.20).

Similarly, dimensionless *external* forces and moments (typically induced by the wind and/or the waves) can be represented by the 4x1 vector

$$\{F\} = \begin{pmatrix} \bar{V}_0^{ext} \\ \bar{M}_0^{ext} \\ \bar{V}_1^{ext} \\ \bar{M}_1^{ext} \end{pmatrix} \tag{2.31}$$

As illustrated in Figure 6, it is important to notice that these forces and moments apply to lumped masses at the boundaries of the beam and are therefore distinct from the *internal* shear forces and moments that can exist within the beam. The $\{F\}$ vector is related to $\{C\}$ by the 4x4 $[S]$ matrix such that

$$\{F\} = [S]\{C\} \tag{2.32}$$

An example of the $[S]$ matrix can be found p.1065 of [1]. The components of $[S]$ can be derived by writing down the equations of motion at the boundaries. In the following section these generalized boundary conditions featuring inertia, damping and stiffness are derived in the frequency domain for the coupled surge/pitch motion. The same methodology can easily be generalized to other degrees of freedom and coupling mechanisms. The added mass terms are not shown here but can readily be added to the inertia terms.

M_1^{ext}

V_1^{ext}

V_1

M_1

V_0

M_0

M_0^{ext}
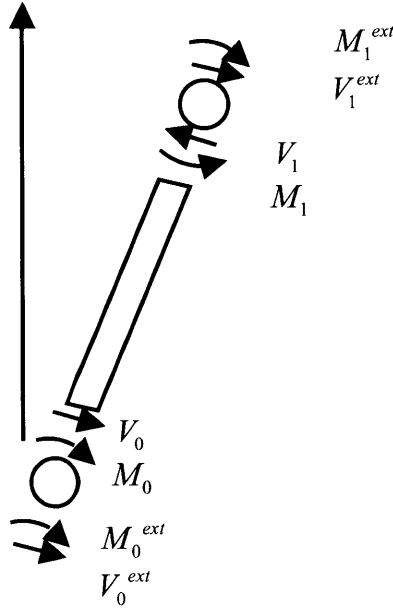
V_0^{ext}

Figure 6: Boundary conditions at the extremities of a block;
All the forces and moments are represented as acting on the lumped masses.

Force balance on the bottom lumped mass

$$(-M_{11}\omega^2 + i\omega B_{11} + C_{11})W_0 + (-M_{15}\omega^2 + i\omega B_{11} + C_{15})\Theta_0 = V_0 + V_0^{ext}(\omega) \qquad (2.33)$$

Using (2.4) to express the shear force as a function of geometric parameters, we obtain

$$(-M_{11}\omega^2 + i\omega B_{11} + C_{11})W_0 + (-M_{15}\omega^2 + i\omega B_{11} + C_{15} + P + GA)\Theta_0 - GAW_0' = V_0^{ext}(\omega) \ (2.34)$$

Moment balance on the bottom lumped mass

$$(-M_{55}\omega^2 + i\omega B_{55} + C_{55})\Theta_0 + (-M_{51}\omega^2 + i\omega B_{51} + C_{51})W_0 = M_0 + M_0^{ext}(\omega) \qquad (2.35)$$

Similarly, using (2.6) to write the bending moment as a function of the curvature, we obtain

$$(-M_{55}\omega^2 + i\omega B_{55} + C_{55})\Theta_0 + (-M_{51}\omega^2 + i\omega B_{51} + C_{51})W_0 - EI\Theta_0' = M_0^{ext}(\omega) \qquad (2.36)$$

Equations (2.34) and (2.36) agree with the ones given p.1064 in [1], but are more general because they include coupling between the various degrees of freedom.

Once again the dimensionless boundary conditions are obtained by dividing the linear momentum equations by GA and the angular momentum equations by EI/L. The dimensionless parameters appearing below are summarized in Table 4.

At the bottom

$$(-\bar{M}_{11}b^2s^2 + ibs\bar{B}_{11} + \bar{C}_{11})\bar{W}_0 + (1 + F^2s^2 - \bar{M}_{15}b^2s^2 + ibs^2\bar{B}_{15} + \bar{C}_{15}s^2)\Theta_0 - \bar{W}_0{'} = \bar{V}_0^{ext}(\omega) \quad (2.37)$$

$$(-\bar{M}_{55}b^2 + ib\bar{B}_{55} + \bar{C}_{55})\Theta_0 + (-\bar{M}_{51}b^2 + ib\bar{B}_{51} + \bar{C}_{51})\bar{W}_0 - \Theta_0{'} = \bar{M}_0^{ext}(\omega) \quad (2.38)$$

At the top

Boundary conditions at the top of a segment can be derived in a similar way by flipping the sign of the internal shear force and bending moment

$$(-\bar{M}_{11}b^2s^2 + ibs\bar{B}_{11} + \bar{C}_{11})\bar{W}_1 + (-1 - F^2s^2 - \bar{M}_{15}b^2s^2 + ibs^2\bar{B}_{15} + \bar{C}_{15}s^2)\Theta_1 + \bar{W}_1{'} = \bar{V}_1^{ext}(\omega) \quad (2.39)$$

$$(-\bar{M}_{55}b^2 + ib\bar{B}_{55} + \bar{C}_{55})\Theta_1 + (-\bar{M}_{51}b^2 + ib\bar{B}_{51} + \bar{C}_{51})\bar{W}_1 + \Theta_1{'} = \bar{M}_1^{ext}(\omega) \quad (2.40)$$

Parameter	Description
$\bar{V}^{ext} = V^{ext}/GA$	Force parameter
$\bar{M}^{ext} = M^{ext}/(EI/L)$	Moment parameter
$\bar{C}_{ij} = C_{ij}/(GA/L) \ i,j=1...3$ $\bar{C}_{ij} = C_{ij}/(EI/L) \ i,j=4...6$ $\bar{C}_{ij} = C_{ij}/(EI/L^2) \ i=1..3, j=4...6$	Stiffness parameter
$\bar{B}_{ij} = B_{ij}/\sqrt{mGA} \ i,j=1...3$ $\bar{B}_{ij} = B_{ij}/\sqrt{mEIL^2} \ i,j=4...6$ $\bar{B}_{ij} = B_{ij}/\sqrt{mEI} \ i=1..3, j=4...6$	Damping parameter
$\bar{M}_{ij} = M_{ij}/mL \ i,j=1...3$ $\bar{M}_{ij} = M_{ij}/mL^3 \ i,j=4...6$ $\bar{M}_{ij} = M_{ij}/mL^2 \ i=1..3, j=4...6$	Inertia parameter

Table 4: Dimensionless parameters used for the boundary conditions in Tower Flex

2.2.4 Application to free vibration

The natural frequencies of the beam are such that there exists a mode shape which

- is different from equilibrium (i.e. a non-zero set of coefficients $\{C\}$)
- satisfies the boundary conditions in displacements, forces or a combination of the two

For a free-free beam such as the TLP without any *external* excitations at the ends, the vibration problem consists in finding the values of ω such that the matrix $S(\omega)$ is singular, which is equivalent to

$$\det S(\omega) = 0 \qquad (2.41)$$

For a beam that is clamped at both ends, the vibration problem is equivalent to

$$\det Z(\omega) = 0 \qquad (2.42)$$

All other cases (pinned-pinned, pinned-free...) can be analyzed by assembling the appropriate matrix that combines rows of $[S]$ and $[Z]$, and then looking for the zeros of its determinant.

2.2.5 Finite blocks model and continuity conditions

If we want to model a beam with non uniform properties, we can divide it into several blocks (or segments) with uniform properties.

For a given block i with uniform properties, the Arboleda model yields two 4x4 matrices $[S_i]$ and $[Z_i]$ that relate the mode shape defined by the 4x1 vector

$$\{C_i\} = \begin{Bmatrix} C_{i1} \\ C_{i2} \\ C_{i3} \\ C_{i4} \end{Bmatrix} \qquad (2.43)$$

to the *external* forces and moments at the boundaries

$$\{F_i\} = \begin{pmatrix} \overline{V}_{i-}^{ext} \\ \overline{M}_{i-}^{ext} \\ \overline{V}_{i+}^{ext} \\ \overline{M}_{i+}^{ext} \end{pmatrix} \qquad (2.44)$$

by

$$\{F_i\} = [S_i]\{C_i\} \qquad (2.45)$$

and to the displacements

$$\{X_i\} = \begin{pmatrix} \overline{w}_{i-} \\ \theta_{i-} \\ \overline{w}_{i+} \\ \theta_{i+} \end{pmatrix} \qquad (2.46)$$

by

$$\{X_i\} = [Z_i]\{C_i\} \qquad (2.47)$$

Now let us consider the case of two different blocks (1 and 2) with uniform properties, for which we would like to obtain the equivalent of the $[S]$ and $[Z]$ matrices to study the vibration problem.

Suppose we know the *external* forces and moments defined in Figure 7

$$\{F^{ext}\} = \begin{pmatrix} \overline{V}_1^{ext} \\ \overline{M}_1^{ext} \\ \overline{V}_2^{ext} \\ \overline{M}_1^{ext} \end{pmatrix} \qquad (2.48)$$

We would like to compute the deflection in each of the two blocks. There are 8 unknowns represented by the 8x1 concatenated vector

$$\{C\} = \begin{pmatrix} C_1 & C_2 \end{pmatrix}^t = (C_{11}...C_{14}\,C_{21}...C_{24})^t \qquad (2.49)$$

Four equations come from the *external* end forces and moments, while the continuity conditions at the interface between the two blocks provide the remaining four equations for the problem:

- Continuity of displacements $w_{1+} = w_{2-}$
- Continuity of rotations $\theta_{1+} = \theta_{2-}$
- Conservation of linear momentum
- Conservation of angular momentum
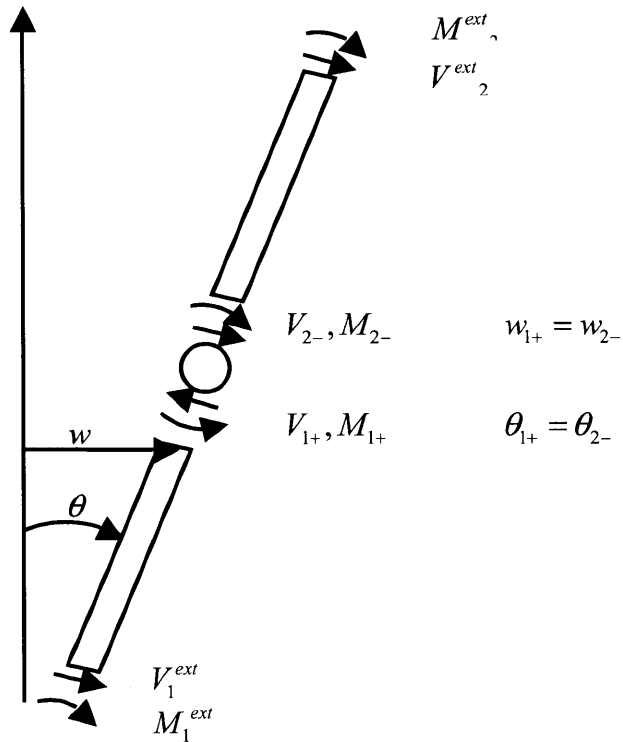
Figure 7: Continuity conditions at the interface between two blocks

The first two conditions are self-explanatory and must hold for the structure to retain its integrity. To understand why there is continuity of rotations rather than slopes, just take a look at the case of pure shear between two blocks with different areas. In that case the continuity of the shear force causes a discontinuity of the shear angle, which is also the slope ($GA_1\gamma_1 = GA_2\gamma_2 \rightarrow \gamma_1 \neq \gamma_2$).

The last two continuity conditions at the interface between two blocks can be determined by making a detailed force and moment balance.

The linear momentum principle for a mass-spring element (m, k) at the interface between two blocks is

$$m\ddot{w} = V_{2-} - V_{1+} - kw \qquad (2.50)$$

Or equivalently

$$m\ddot{w} + kw - \Delta V = 0 \tag{2.51}$$

However in Tower Flex the upper block sees the mass as a boundary condition at its bottom end

$$m\ddot{w} = V_{2-} - kw \tag{2.52}$$

Or equivalently

$$m\ddot{w} + kw - V_{2-} = 0 \tag{2.53}$$

A similar equation holds for the lower block with a change in sign for the shear force

$$m\ddot{w} + kw + V_{1+} = 0 \tag{2.54}$$

Therefore to ensure that the correct linear momentum equation (2.51) is satisfied, we must *add* the two left-hand sides of equations (2.53) and (2.54) while making sure that we do not count the mass and stiffness twice. The conservation of angular momentum is enforced similarly.

2.2.6 Implementation

All the continuity conditions must be carefully enforced because there is continuity of the physical quantities, not of the dimensionless ones. Therefore dimensionless quantities (and corresponding equations) need to be rescaled accordingly

$$\begin{cases} w \to w \times L \\ \theta \to \theta \\ V \to V \times GA_s \\ M \to M \times EI \,/\, L \end{cases} \tag{2.55}$$

Each of these equations can be written by "extracting" the appropriate 1x4 rows R_j of the $[S_i]$ and $[Z_i]$ matrices.

For instance, $w_{1+} = w_{2-}$ is equivalent to $\left(R_3(Z_1) \times L_1 \right) C = \left(R_1(Z_2) \times L_2 \right) C$, which can be rewritten as the homogeneous equation

$$\left(R_3(Z_1) \times L_1 - R_1(Z_2) \times L_2 \right) C = 0 \tag{2.56}$$

33

A similar equation can be derived for the rotation angles.

For the conservation of linear and angular momentum, the following remarks apply:

- The appropriate rows of [S] are added to ensure the correct force and moment balance. In the absence of mass or springs, there is continuity of the shear force and the bending moment, but this is not true in general.

- The generalized boundary conditions at an interface (mass, damping and stiffness terms) need only be accounted for *one* of the two blocks. In Tower Flex they are generally implemented at the upper block as a bottom end boundary condition (this is because the solution is easier to write at $z=0$ than at $z=L$).

Eventually we obtain the following linear system expressed in matrix form

$$
\begin{pmatrix}
R_1(S_1) & (0) \\
R_2(S_1) & (0) \\
R_3(S_1) \times GA_1 & R_1(S_2) \times GA_2 \\
R_4(S_1) \times EI_1 / L_1 & R_2(S_2) \times EI_2 / L_2 \\
R_3(Z_1) \times L_1 & -R_1(Z_2) \times L_2 \\
R_4(Z_1) & -R_2(Z_2) \\
(0) & R_3(S_2) \\
(0) & R_4(S_2)
\end{pmatrix}
\begin{pmatrix}
C_{11} \\
C_{12} \\
C_{13} \\
C_{14} \\
C_{21} \\
C_{22} \\
C_{23} \\
C_{24}
\end{pmatrix}
=
\begin{pmatrix}
\overline{V}_1^{ext} \\
\overline{M}_1^{ext} \\
0 \\
0 \\
0 \\
0 \\
\overline{V}_2^{ext} \\
\overline{M}_2^{ext}
\end{pmatrix}
\qquad (2.57)
$$

This 8x8 matrix is a generalized [S] matrix such that $\{M\}=[S]\{C\}$. The natural frequencies are the frequencies for which there exists $\{C\}\neq 0$ such that $[S]\{C\}=0$. Therefore they can be found by setting the determinant of [S] to zero.

This method can easily be extended to an arbitrary number N of blocks subject to continuity conditions. In the general case, [S] and [Z] will be 4Nx4N matrices with $\underbrace{4\times4}_{\text{boundaries}} + 8\times4 \underbrace{(N-1)}_{\text{\# of interfaces}} = 32N - 16$ non-zero elements.

The sparse properties of these matrices make it easy to compute their determinant or inverse in MATLAB ©.

2.3 3D Tower Flex

2.3.1 Motivation

In the previous section, we have modeled the flexural motion of a beam using two continuous parameters (one translation and one rotation). We call this planar model 2D Tower Flex. It allows us to understand the behavior of the floating wind turbine in each of the two vertical planes passing through the tower axis:

- fore-aft (surge and pitch)
- side-to-side (sway and roll)

Yet in a realistic model of a floating wind turbine we need to account for all degrees of freedom and cross-coupling between them, which can come from:

- the mooring lines
- the turbine
- wind and waves coming from different directions

Following these observations we have extended 2D Tower Flex into 3D Tower Flex, a coupled frequency-domain model that simulates the motion of the floating wind turbine in three dimensions.

Table 5 below summarizes the different degrees of freedom (DOFs) in 3D Tower Flex. The four DOFs mentioned above are flexural. Due to the stiff nature of the tower in heave and yaw, we do not expect significant deformations along these dimensions therefore the corresponding DOFs are assumed to be rigid.

Index	Degree of freedom (DOF)	Type of motion
1	Surge	Flexural
2	Sway	Flexural
3	Heave	Rigid
4	Roll	Flexural
5	Pitch	Flexural
6	Yaw	Rigid

Table 5: Degrees of freedom (DOFs) for the tower in 3D Tower Flex

Single block with uniform properties

The "semi-flexural" motion of beam with uniform properties can be described by
- 4 coefficients $C_1 \ldots C_4$ for surge and pitch
- 4 coefficients $C_5 \ldots C_8$ for sway and roll
- 1 coefficient C_9 for heave
- 1 coefficient C_{10} for yaw

These 10 coefficients are concatenated in a 10x1 vector

$$\{C\} = (C_1 \ldots C_{10})^t \qquad (2.58)$$

Equations of motion

The flexural equations of motion in surge/pitch and sway/roll are continuous and lead to identical differential equations (2.15). Furthermore since the tower is axisymmetric they have exactly the same coefficients. The only way the motions in these two planes can be different is through different boundary conditions.

In practice though, the relative orientation of sway and roll differs from that of surge and pitch on which 2D Tower Flex is based. As illustrated in Table 6, this is equivalent to changing θ into $-\theta$ for the sway angle.

Surge-pitch (1-5) (as in 2D Tower Flex)	Sway-roll (2-4)
  5	 4
M and V have the same direction $\gamma = w' - \theta$ Contribution of weight to shear $+P\theta$ Shear force equation $V + P\theta = GA\gamma$ $V = GAw' - (GA + P)\theta$	M and V have opposite direction $\gamma = w' + \theta$ Contribution of weight to shear $-P\theta$ Shear force equation $V - P\theta = GA\gamma$ $V = GAw' + (GA + P)\theta$

Table 6: Orientations of flexural DOFs in 3D Tower Flex

The equations of motion for heave and yaw are simply the rigid body equations written at the center of gravity of each block.

Just like in 2D Tower Flex, the $[S]$ and $[Z]$ matrices relate the mode shape defined by $\{C\}$ respectively to:

- the *external* forces and bending moments at the boundaries

$$\{F\} = \left(\begin{array}{cccccccccc} \overline{F}_{1-}^{ext} & \overline{F}_{2-}^{ext} & \overline{F}_{4-}^{ext} & \overline{F}_{5-}^{ext} & \overline{F}_{1+}^{ext} & \overline{F}_{2+}^{ext} & \overline{F}_{4+}^{ext} & \overline{F}_{5+}^{ext} & \overline{F}_{3}^{ext} & \overline{F}_{6}^{ext} \end{array}\right)^t \quad (2.59)$$

- the displacements and rotations at the boundaries

$$\{X\} = \left(\begin{array}{cccccccccc} \overline{X}_{1-} & \overline{X}_{2-} & \overline{X}_{4-} & \overline{X}_{5-} & \overline{X}_{1+} & \overline{X}_{2+} & \overline{X}_{4+} & \overline{X}_{5+} & \overline{X}_{3} & \overline{X}_{6} \end{array}\right)^t \quad (2.60)$$

The force matrix $[S]$ is such that $\{F\} = [S]\{C\}$ and the displacement matrix $[Z]$ is such that $\{X\} = [Z]\{C\}$. Note that for consistency all generalized forces (i.e. forces and moments) are denoted by F, and all generalized displacements (i.e. displacements and rotations) are denoted by X, where the subscript helps to understand the corresponding DOF.

The $[Z]$ matrix shown in Figure 8 (where R denotes a 1x4 row) is a straightforward extension of the 2D $[S]$ matrices obtained in each plane:

- Fore-aft (FA) for surge and pitch
- Side-to-side (STS) for sway and roll

$$\begin{pmatrix} R_1(Z_{FA}) & (0) & 0 & 0 \\ (0) & R_1(Z_{STS}) & 0 & 0 \\ (0) & R_2(Z_{STS}) & 0 & 0 \\ R_2(Z_{FA}) & (0) & 0 & 0 \\ R_3(Z_{FA}) & (0) & 0 & 0 \\ (0) & R_3(Z_{STS}) & 0 & 0 \\ (0) & R_4(Z_{STS}) & 0 & 0 \\ R_4(Z_{FA}) & (0) & 0 & 0 \\ (0) & (0) & 1 & 0 \\ (0) & (0) & 0 & 1 \end{pmatrix} \begin{pmatrix} C_1 \\ C_2 \\ C_3 \\ C_4 \\ C_5 \\ C_6 \\ C_7 \\ C_8 \\ C_9 \\ C_{10} \end{pmatrix} = \begin{pmatrix} \overline{X}_{1-} \\ \overline{X}_{2-} \\ \overline{X}_{4-} \\ \overline{X}_{5-} \\ \overline{X}_{1+} \\ \overline{X}_{2+} \\ \overline{X}_{4+} \\ \overline{X}_{5+} \\ \overline{X}_{3} \\ \overline{X}_{6} \end{pmatrix}$$

Figure 8: Z matrix in 3D Tower Flex for a single block

Without cross-coupling (other than that existing between surge and pitch, as well as sway and roll), the $[S]$ matrix shown in Figure 9 is also a straightforward extension of the 2D $[S]$ matrices obtained in each plane

$$
\begin{pmatrix}
R_1(S_{FA}) & (0) & 0 & 0 \\
(0) & R_1(S_{STS}) & 0 & 0 \\
(0) & R_2(S_{STS}) & 0 & 0 \\
R_2(S_{FA}) & (0) & 0 & 0 \\
R_3(S_{FA}) & (0) & 0 & 0 \\
(0) & R_3(S_{STS}) & 0 & 0 \\
(0) & R_4(S_{STS}) & 0 & 0 \\
R_4(S_{FA}) & (0) & 0 & 0 \\
(0) & (0) & \text{rigid heave} & 0 \\
(0) & (0) & 0 & \text{rigid sway}
\end{pmatrix}
\begin{pmatrix}
C_1 \\ C_2 \\ C_3 \\ C_4 \\ C_5 \\ C_6 \\ C_7 \\ C_8 \\ C_9 \\ C_{10}
\end{pmatrix}
=
\begin{pmatrix}
\bar{F}_{1-}^{ext} \\ \bar{F}_{2-}^{ext} \\ \bar{F}_{4-}^{ext} \\ \bar{F}_{5-}^{ext} \\ \bar{F}_{1+}^{ext} \\ \bar{F}_{2+}^{ext} \\ \bar{F}_{4+}^{ext} \\ \bar{F}_{5+}^{ext} \\ \bar{F}_{3}^{ext} \\ \bar{F}_{6}^{ext}
\end{pmatrix}
$$

Figure 9: S matrix in 3D Tower Flex for a single block without cross-coupling

A more general version of $[S]$ taking into account cross-coupling from 6x6 stiffness and mass matrices is shown in Figure 10

$$
\begin{pmatrix}
R_1(S_{FA}) & \times & \times & \times \\
\times & R_1(S_{STS}) & \times & \times \\
\times & R_2(S_{STS}) & \times & \times \\
R_2(S_{FA}) & \times & \times & \times \\
R_3(S_{FA}) & \times & \times & \times \\
\times & R_3(S_{STS}) & \times & \times \\
\times & R_4(S_{STS}) & \times & \times \\
R_4(S_{FA}) & \times & \times & \times \\
 & \text{rigid} & \text{heave} & \\
 & \text{rigid} & \text{sway} &
\end{pmatrix}
\begin{pmatrix}
C_1 \\ C_2 \\ C_3 \\ C_4 \\ C_5 \\ C_6 \\ C_7 \\ C_8 \\ C_9 \\ C_{10}
\end{pmatrix}
=
\begin{pmatrix}
\bar{F}_{1-}^{ext} \\ \bar{F}_{2-}^{ext} \\ \bar{F}_{4-}^{ext} \\ \bar{F}_{5-}^{ext} \\ \bar{F}_{1+}^{ext} \\ \bar{F}_{2+}^{ext} \\ \bar{F}_{4+}^{ext} \\ \bar{F}_{5+}^{ext} \\ \bar{F}_{3}^{ext} \\ \bar{F}_{6}^{ext}
\end{pmatrix}
$$

Figure 10: S matrix in 3D Tower Flex for a single block with cross-coupling

The coefficients can be determined by writing the equations of motion at the boundary conditions as explained in paragraph 2.2.3. The equations for these generalized boundary

conditions have been treated analytically using MATLAB's © symbolic computation engine (MUPAD) and are all on file.

2.3.2 Finite blocks model and continuity conditions

Continuity conditions

For the flexural DOFs, the same continuity conditions apply at the interface between two blocks j and $j+1$:

- Continuity of displacements and rotations

$$X_{i+}^{j} = X_{i-}^{j+1}, i = 1,2,4,5 \tag{2.61}$$

- Conservation of linear momentum in surge and sway

- Conservation of angular momentum in roll and pitch

Overall, there are 8 continuity conditions for the flexural DOFs.

For the rigid DOFs, the equations of motion for each block are added together to cancel the internal forces out and obtain the equations of motion for the entire structure.

Assembly of S and Z matrices

The method to assemble the matrices from individual blocks is similar to that of 2D Tower Flex as described in 2.2.6., except for the following points:

- The dimensions of [S] and [Z] matrices are now ($8N$+2) x ($8N$+2) (8 coefficients for the flexural motion of each of the N tower blocks plus two rigid DOFs for the entire structure)

- For the heave motion the length of first block is arbitrarily taken as the reference for dimensionless quantities, therefore the corresponding column of [S] and [Z] matrices (corresponding to heave) must be rescaled by *L(1)/L(i)*

2.4 Description of the braces

This section provides a description of the braces and their modeling in 3D Tower Flex.

2.4.1 Coordinate systems

Figure 11 shows a top view of the braces labeled from 1 to 3. Also shown is the horizontal projection of the global coordinate system with its origin at the center of section C. Each brace is oriented at an angle θ (positive counterclockwise) with the surge axis.
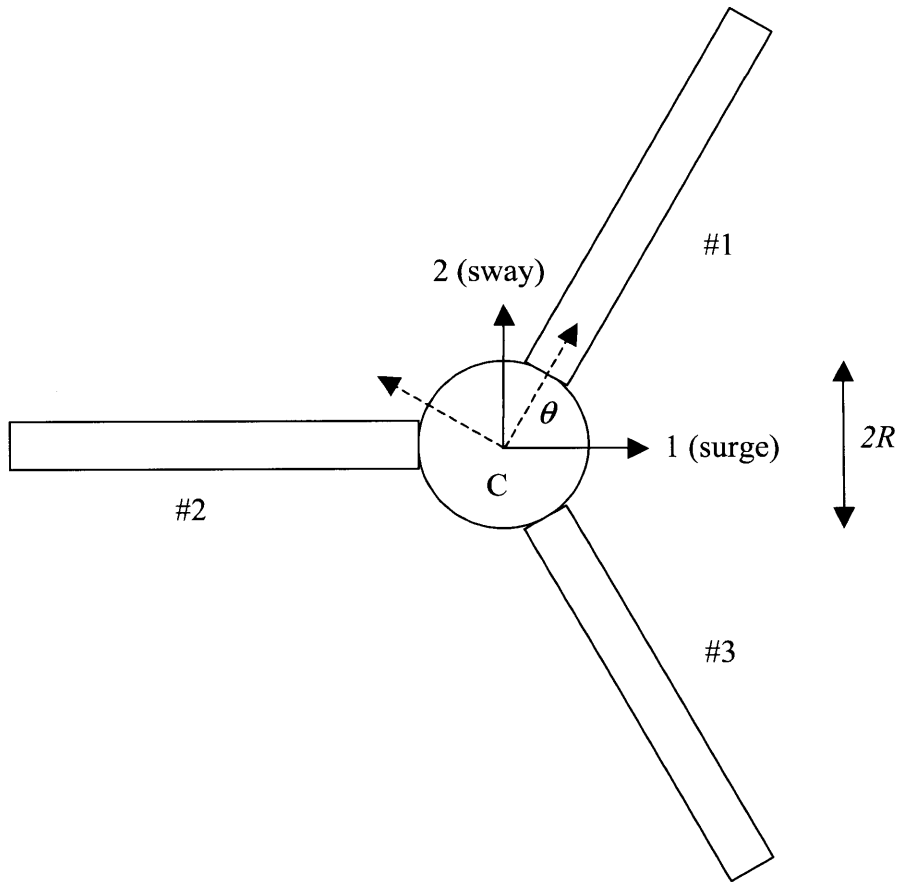
Figure 11: Top view of the braces

Figure 12 is a side view of the braces showing the global coordinate system with its origin at the center of section C.
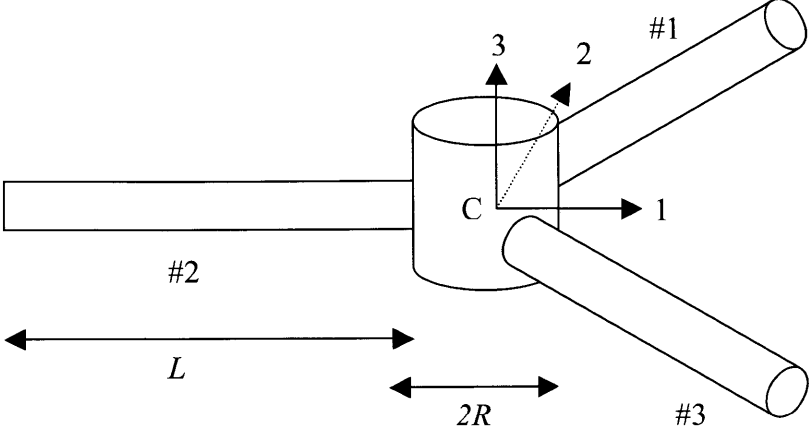
Figure 12: Side view of the braces

Figure 13 shows the local earth-fixed reference frame used to describe the motion of the brace. The corresponding local coordinate system is obtained by rotating the global coordinate system by an angle θ in the counter-clockwise direction and defining its origin as the location of the brace root at rest.
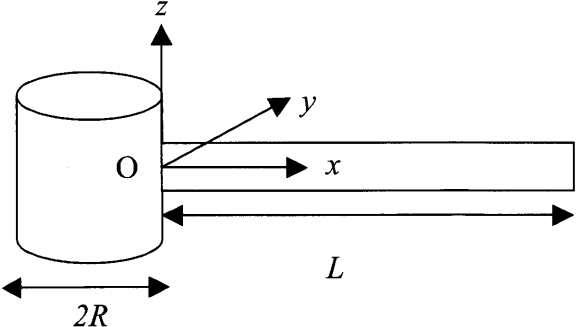
Figure 13: Local coordinate system for one brace

2.4.2 Degrees of freedom

Each brace is modeled exactly like a tower segment with

- Two bending planes xz (vertical) and xy (horizontal)

    - in the vertical plane, x and θ_y have the same orientation as sway/roll
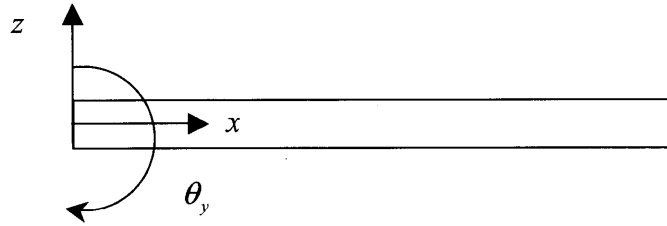
- in the horizontal plane, y and θ_z have the same orientation as surge/pitch
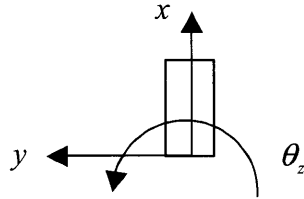
- A rigid axial displacement along x axis
- A rigid rotation about x axis (similar to yaw for the tower)

The same routines used to code for the tower blocks are used to code for the braces, with the following correspondence between the DOFs.

Tower	1 Surge	2 Sway	3 Heave	4 Roll	5 Pitch	6 Yaw
Brace	y	z	x	θ_y	θ_z	θ_x

Table 7: Equivalence between the DOFs of the tower and the braces

2.4.3 Boundary conditions

"Free" conditions at the brace tip with restoring effects from the mooring lines

Since no moments are exerted at the brace tip, the $\mathbf{C}^{\text{LINES}}$ matrix only has translational components.

"Clamped" conditions at the brace root

The forces and moments at the brace root given by the [S] matrix are added to the equations of motion at the interface between two tower blocks.

- *xz* (vertical bending): V_z adds to the heave rigid motion and creates a moment $-RV_z$ about the center of the section that adds to the M_y moment.

- *xy* (horizontal bending): V_y adds to the surge/sway equations of motion and creates a yaw moment RV_y about the center of the section that adds to the M_z moment.

- Rigid DOFs: the axial force F_x passes through the center of the section and only affects the equations of motion in surge and sway. The torsion moment M_x adds to the roll and pitch moments.

- In the global coordinate system, the equivalent surge, sway, heave, roll, pitch and yaw excitations are applied to the tower

$$F_1 = F_x \cos\theta - V_y \sin\theta$$
$$F_2 = F_x \sin\theta + V_y \cos\theta$$
$$F_3 = V_z$$
$$F_4 = M_x \cos\theta - (M_y - RV_z)\sin\theta \tag{2.62}$$
$$F_5 = M_x \sin\theta + (M_y - RV_z)\cos\theta$$
$$F_6 = M_z + RV_y$$

Continuity of displacements

The continuity of displacements is enforced at each one of the brace roots assuming small rotations of the tower section in the global coordinate system

$$X_1 - R\sin\theta X_6 = \Delta_x \cos\theta - \Delta_y \sin\theta$$
$$X_2 + R\cos\theta X_6 = \Delta_x \sin\theta + \Delta_y \cos\theta$$
$$X_3 + R\sin\theta X_4 - R\cos\theta X_5 = \Delta_z$$
$$X_4 = \theta_x \cos\theta - \theta_y \sin\theta$$
$$X_5 = \theta_x \sin\theta + \theta_y \cos\theta$$
$$X_6 = \theta_z$$

(2.63)

2.4.4 Implementation

The individual [S] and [Z] matrices for each brace are assembled exactly like for the tower. The generalized [S] matrix is then assembled by blocks with the different [S] matrices from the tower and the braces, and the continuity conditions are then enforced at the appropriate rows as discussed in section 2.2.6. If *Nt* is the number of blocks for the {tower+transition piece} set and *Nb* the number of blocks used to model each of the three braces, then the size of [S] is 8*Nt*+2+3(8*Nb*+2).

Figure 14 shows the structure of this generalized [*S*] matrix with *Nt*=20 and *Nb*=1. As usual, the main diagonal contains the continuity conditions at the interface between blocks, while the off-diagonal elements correspond to the clamped conditions between the braces and the tower described above.
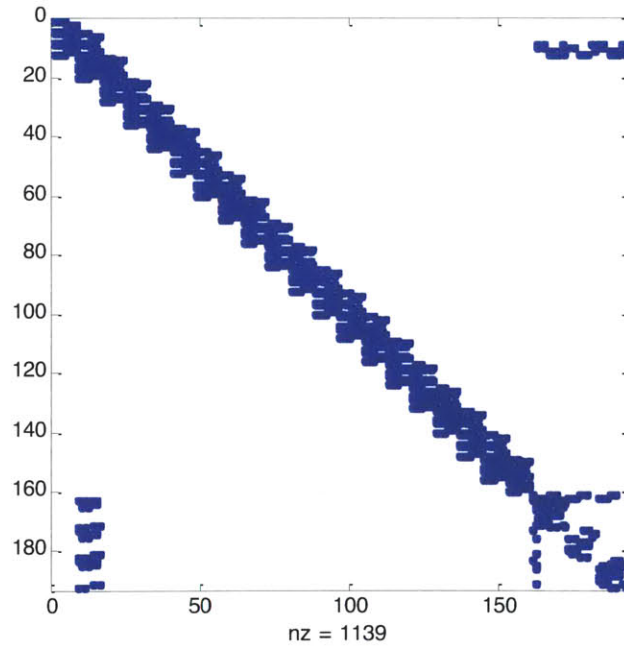
Figure 14: Non-zero elements of the generalized [S] matrix for the {tower + braces} structure

44

2.5 Modeling of the TLP in Tower Flex

This section explains how the different parts of the TLP structure are modeled in Tower Flex as summarized in Figure 15.
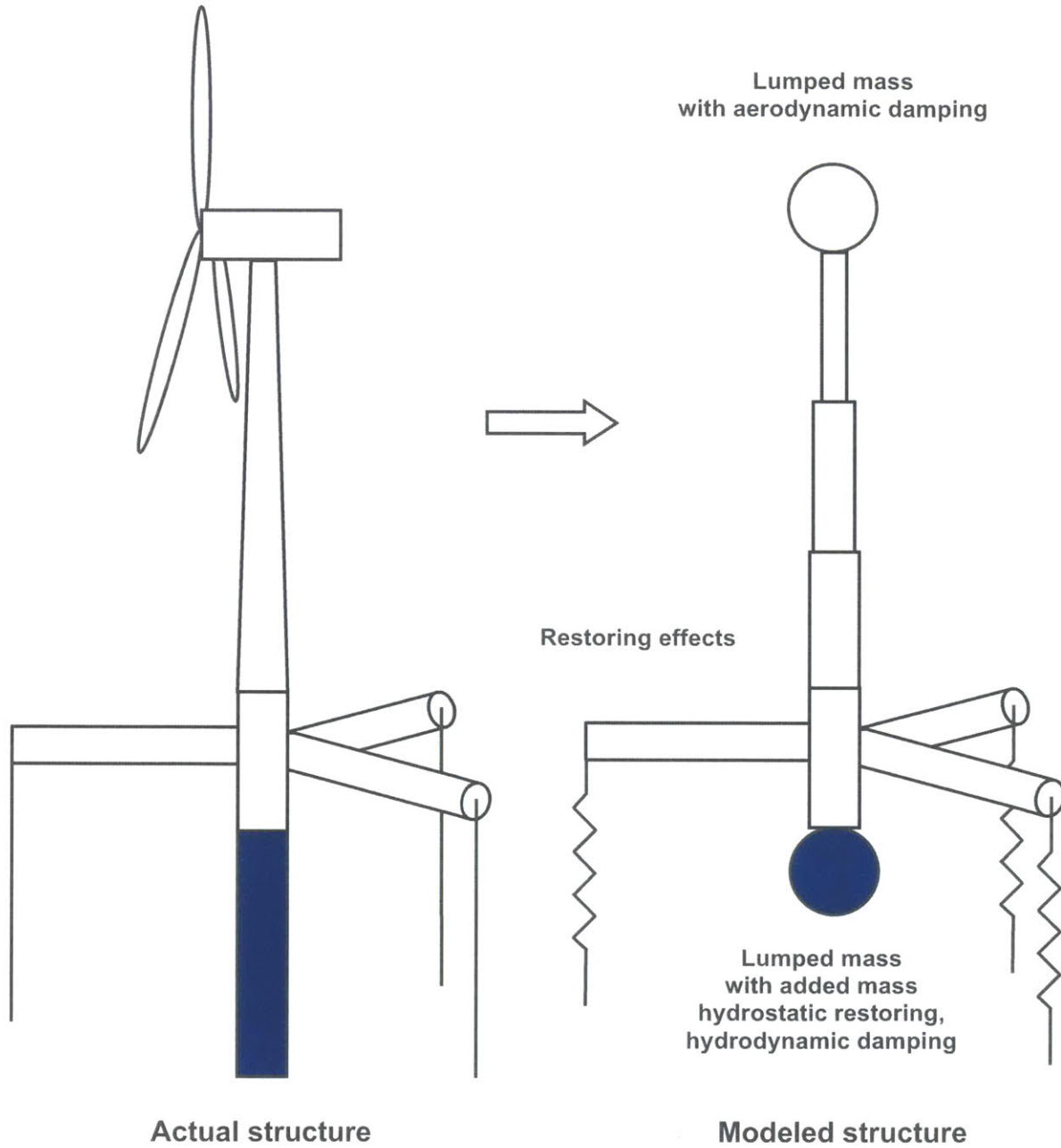
Figure 15: Structural model of the TLP in Tower Flex

2.5.1 Tower and transition piece

They are modeled by a series of 20 blocks with uniform circular hollow cross-section. The following properties are used for a cross-section of radius R and thickness t.

Gross area

$$A_g = \iint dA = 2\pi R t \tag{2.64}$$

Polar moment of inertia (in-plane)

$$I = \iint x^2 \, dA = \iint y^2 \, dA = \pi R^3 t \tag{2.65}$$

Mass moment of inertia (in-plane)

$$J = \rho I \tag{2.66}$$

Shear coefficient

$$k = \frac{2(1+v)}{4+3v} \tag{2.67}$$

according to [2] although $k = \dfrac{2(1+v)}{4+2v} = \dfrac{1+v}{2+v}$ can also be found in the literature [3].

2.5.2 Braces and mooring lines

Each of the braces is modeled as a uniform steel beam with a circular hollow cross-section clamped to the tower at its root and connected to the mooring lines at its tip (see paragraph 2.4). In the present work, the mooring lines are considered to be without mass and do not participate in the dynamics except through their restoring effects.

Throughout this work the following properties are used for steel:

	Density [kg/m3]	**7,850**
Steel properties	Young's modulus [GPa]	**210**
	Poisson's ratio	**0.3**

Table 8: Properties of steel used in Tower Flex

2.5.3 Buoy

The steel buoy is modeled as a rigid lumped mass connected to the transition piece right below the free surface. The 6x6 mass, added mass, hydrodynamic damping and hydrostatics restoring matrices are applied as boundary conditions at the bottom of the transition piece.

Figure 16 below shows the non-zero components of the frequency-dependent added-mass matrix calculated by WAMIT©. Since the buoy is axisymmetric, only the surge/pitch components A_{11}, A_{33}, A_{15} and A_{55} as well as the heave component A_{33} are shown. Note that the added mass of the buoy in heave is roughly equal to that of the buoy itself, while the added mass in surge and sway is an order of magnitude higher.
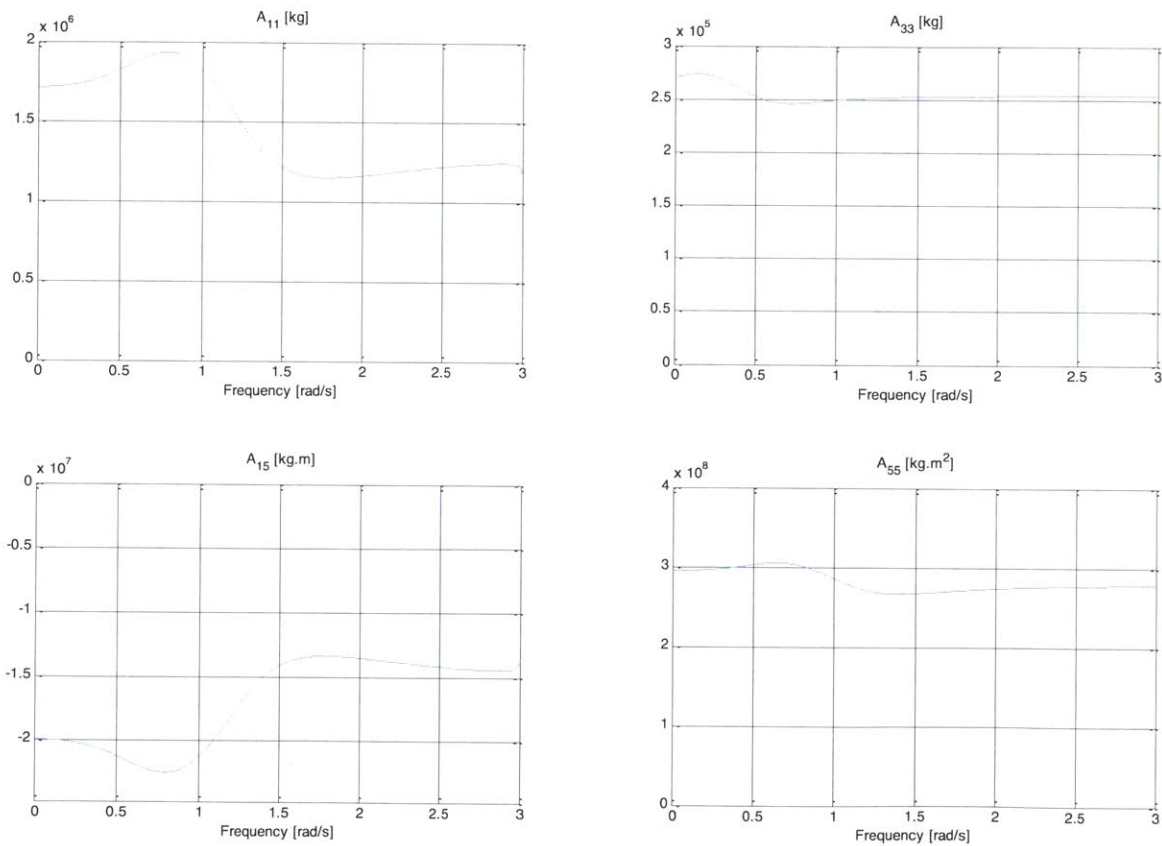
Figure 16: Added mass properties of the TLP

Similarly, Figure 16 shows the non-zero components of the frequency-dependent hydrodynamic damping matrix calculated by WAMIT© as a function of frequency. Hydrodynamic damping vanishes at low and high frequencies but effectively contributes to the damping of the structure at pitch resonance (see Chapter 4).
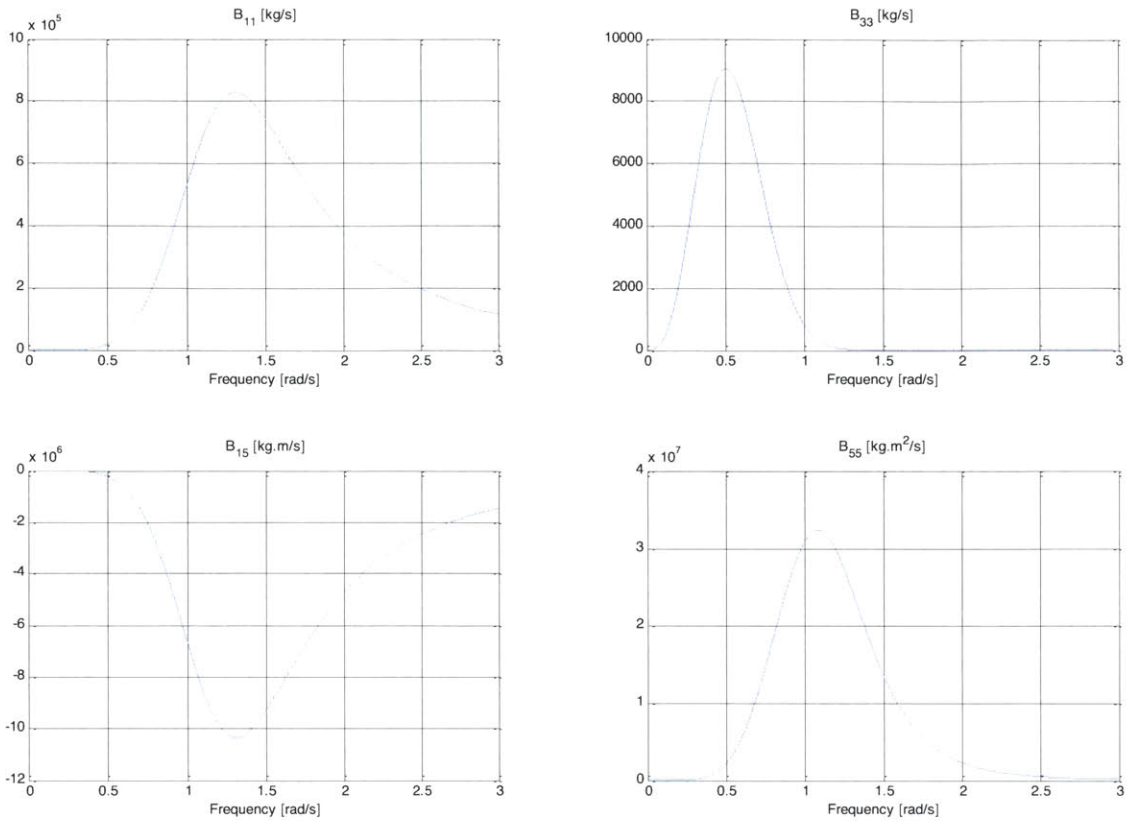
Figure 17: Hydrodynamic damping properties of the TLP

2.5.4 Tower head

The entire {blades+hub+nacelle} structure is modeled as a lumped mass rigidly connected to the top of tower, where the 6x6 mass and aerodynamic damping matrices are applied as boundary conditions.

Aerodynamic damping

For the aerodynamic damping, the values of B_{11}^{AERO}, B_{22}^{AERO} and B_{66}^{AERO} are tuned to obtain damping ratios of 6%, 2% and 3% in the fore-aft, side-to-side and yaw modes respectively. These damping ratios are estimated using the half-bandwidth method on motion responses assuming a locally 1-DOF, lightly damped system [4].

Gyroscopic effect

The coupling between the spinning motion of the rotor and the pitch motion of the nacelle (coming from the rotation of the platform or the deflection of the tower) creates a gyroscopic yaw moment defined by

$$F_{6\,gyro} = \dot{X}_5 \times J_{rot}\dot{\alpha} \qquad (2.68)$$

where J_{rot} is the moment of inertia of the spinning rotor, $\dot{\alpha}$ the angular velocity of the rotor (as given by its RPM) and $\dot{X}_5$ the angular velocity of the nacelle pitch motion. This gyroscopic effect is equivalent to an aerodynamic damping term B_{65}^{AERO} that is applied to the top of the tower. Conversely, the coupling between the spinning rotor and the yaw motion of the nacelle induces a pitch moment on the nacelle, which is modeled by an equivalent aerodynamic damping term

$$B_{56}^{AERO} = -B_{65}^{AERO} \qquad (2.69)$$

3 Natural Frequencies

3.1 Case of the rigid TLP

The natural frequencies of the rigid system can be easily obtained by solving the following eigenvalue problem

$$[-\omega^2(\mathbf{A}(\omega)+\mathbf{M})+\mathbf{C}]\mathbf{X}=0 \qquad (3.1)$$

The results for the rigid TLP at rest (no mean wind) are listed in Table 9 below and are compared to the natural frequencies obtained by running Tower Flex with a very high stiffness ($E \rightarrow \infty$) to "force" the rigid body motion.

Mode	Rigid body theory	Tower Flex ($E \rightarrow \infty$)
Surge	0.028	0.028
Sway	0.028	0.028
Heave	2.260	2.260
Roll	0.390	0.390
Pitch	0.391	0.391
Yaw	0.123	0.123

Table 9: Natural frequencies (in Hz) of the rigid TLP without mean wind

In the absence of mean wind, the mooring system is symmetric so that the surge/sway and pitch/roll modes are virtually identical, with pitch and roll differing only slightly because of the higher inertia of the rotor in roll. The results also show a perfect agreement between Tower Flex and the rigid body theory, which serves as a first validation of Tower Flex.

3.2 Case of the flexible TLP

3.2.1 No mean wind

The natural frequencies of the flexible system are then calculated using Tower Flex with the standard value of the steel's Young's modulus presented in Table 8 (E=210 GPa). The results are compared to the natural frequencies of the rigid structure and shown in Table 10 below.

Mode	Tower Flex ($E \to \infty$)	Tower Flex (Finite E)	Relative difference
Surge	0.028	0.028	<0.1%
Sway	0.028	0.028	<0.1%
Heave	2.260	2.187	3.2%
Roll – STS 1	0.390	0.268	31.3%
Pitch – FA 1	0.391	0.270	30.9%
Yaw	0.123	0.123	<0.1%
FA 2	-	0.901	-
STS 2	-	0.877	-

Table 10: Natural frequencies (in Hz) of the TLP without mean wind

Comparing the two columns of Table 10, we conclude that the heave and yaw modes are barely affected by the flexibility of the braces (as a reminder, the tower is rigid in heave and yaw). For these modes, the flexibility essentially comes from the mooring lines which make up the "soft" part of the system. Likewise, the surge and sway modes are the same as in the rigid body case.
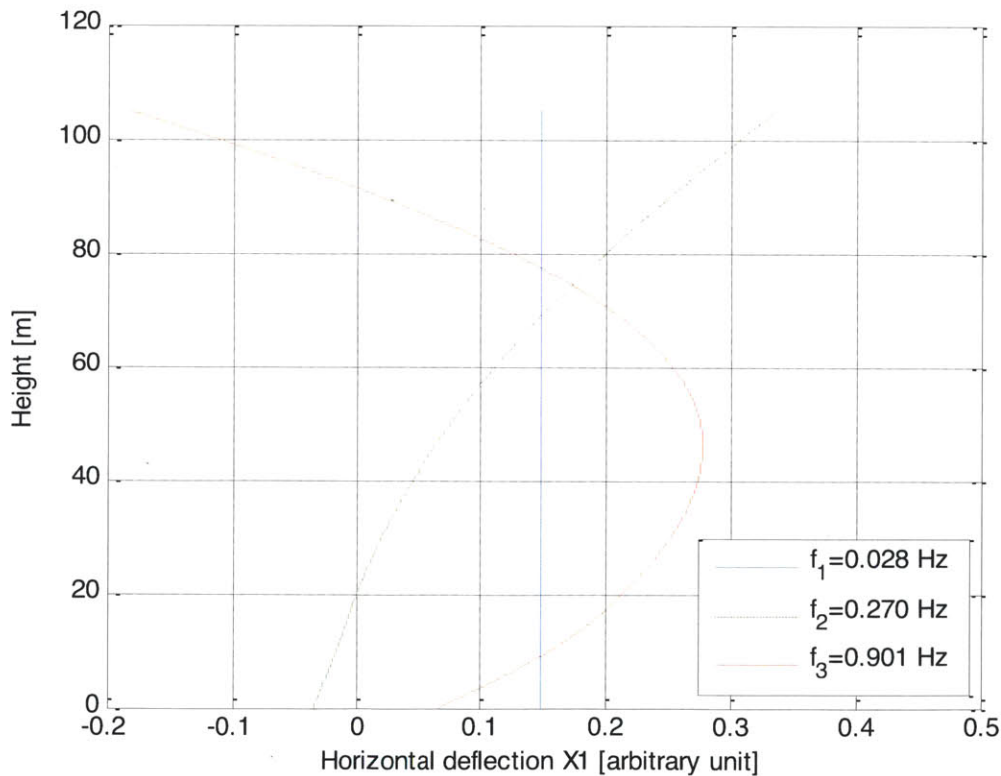
Figure 18: Surge and fore-aft mode shapes of the flexible TLP

51

The finite stiffness of the tower – and to a much lesser extent, that of the braces – manifests itself in the fore-aft (FA) and side-to-side (STS) modes. The flexural motion of the tower is coupled to the oscillations of the mooring lines so that the fundamental frequency for these modes is significantly lower than in the rigid body case. The TLP also exhibits a series of higher natural frequencies that are typical of a continuous vibrating system. Figure 18 above shows a plot of the surge and first two fore-aft mode shapes, where it is clear that the tower is rigid in the surge mode and flexible in the fore-aft modes.

3.2.2 With mean wind

In a more realistic situation, the natural frequencies of the TLP have been calculated at its offset position under a mean wind speed of U=11 m/s. The results are compared to the natural frequencies without wind and shown in Table 11 below.

Mode	No mean wind	Mean wind (11 m/s)	Relative difference
Surge	0.028	0.028	<0.1%
Sway	0.028	0.026	7.1%
Heave	2.187	2.184	0.1%
Roll – STS 1	0.268	0.303	13.1%
Pitch – FA 1	0.270	0.269	0.4%
Yaw	0.123	0.103	16.3%
FA 2	0.901	0.900	0.1%
STS 2	0.877	0.882	0.6%

Table 11: Natural frequencies (in Hz) of the flexible TLP under different wind conditions

The mean offset position of the TLP under a mean wind speed changes the geometry of the mooring lines which are now at an angle and have different restoring properties. To draw an analogy with quantum mechanics, this tends to "break" the symmetry and "split" the frequencies between the fore-aft and side-to-side modes. Indeed, while the natural frequencies in the surge, pitch and heave modes are barely changed, the sway, roll and yaw modes are affected by the offset. The sway natural frequency is now smaller than the surge natural frequency, while the side-to-side modes have higher frequencies. This is especially true for the first side-to-side mode, which mostly depends on the stiffness of the mooring lines than the second side-to-side mode, which mostly depends on the stiffness of the tower. Another remarkable effect is the shift towards lower values of the yaw natural frequency.

An elegant way of visualizing the natural frequencies of the system, proposed by Finn Gunnar Nielsen, Chief Researcher at Statoil, is shown in Figure 19. In this plot, natural frequencies of the TLP at rated wind speed are placed on logarithmic scale along with the excitation spectrum due to the wind, the waves as well as the 1P and 3P blade passing frequencies.
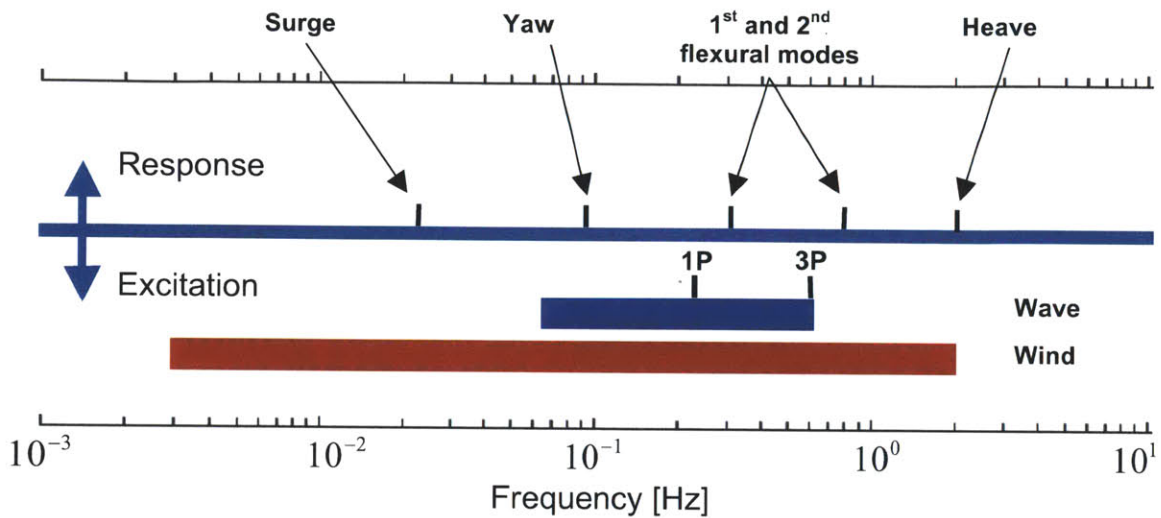
Figure 19: Excitation and response spectra of the TLP at rated wind speed

4 Motion and Tension Response

4.1 Wave forces

Figure 20 below shows the modulus of hydrodynamic surge, heave and pitch forces acting on the buoy for a unit wave amplitude propagating along the surge axis as calculated by WAMIT©. In accordance with linear wave theory [5], the heave force is non-zero at low frequencies, where the surge and pitch excitations vanish. At high frequencies, all excitations vanish. Although phases are not shown here, is it worth mentioning that the heave force is in phase with the wave elevation, while the surge force is 90 degrees ahead of the wave elevation.
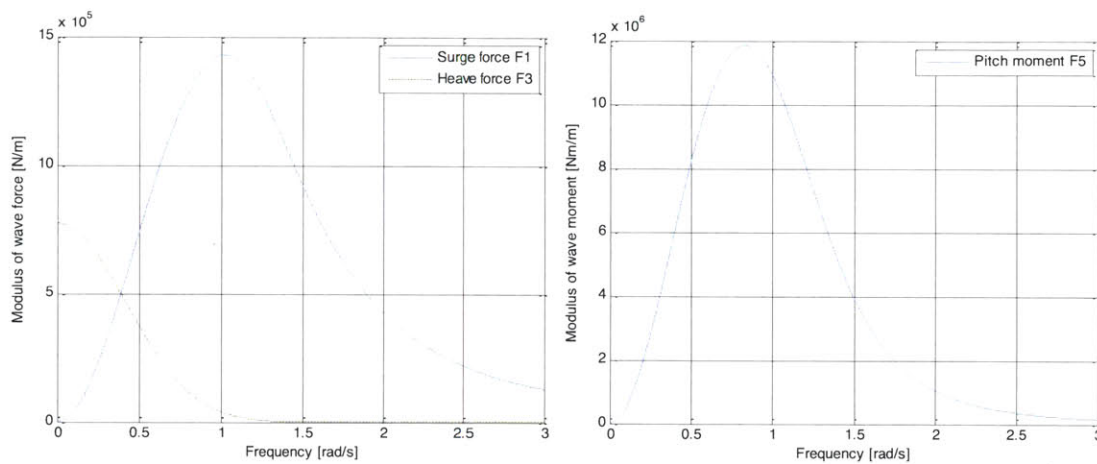
Figure 20: Hydrodynamic waves forces and moments on the TLP

4.2 RAOs for the flexible TLP

Figure 21 to Figure 23 show the six motion RAOs at the free surface and the tension RAOs for each of the three braces obtained with Tower Flex. In each figure, the response to a unit wave amplitude is plotted along with the sea spectrum for a sea state with Hs=10m calculated according to Eq. (4.2) and the 1P blade passing frequency band.

To identify resonance peaks more easily, the natural frequencies (in Hz and rad/s) of the flexible TLP at rated wind speed are reminded below.

Mode	Frequency [Hz]	Frequency [rad/s]
Surge	0.028	0.175
Sway	0.026	0.162
Heave	2.184	13.742
Roll – STS 1	0.303	1.906
Pitch – FA 1	0.269	1.693
Yaw	0.103	0.648
FA 2	0.900	5.663
STS 2	0.882	5.550

Table 12: Natural frequencies of the flexible TLP at rated wind speed

Figure 21 illustrates some of the key design aspects of the TLP in the absence of wind. Under these conditions, the mooring lines are vertical and the only non-zero responses are in surge, heave and pitch. The surge resonance falls mostly outside of the sea spectrum, while the pitch resonance is located far enough (>10%) from the maximum 1P blade passing frequency. Furthermore, there is no resonance in heave because the heave force is zero at the heave natural frequency.

Under a mean wind speed of 7 m/s and 11 m/s, the response of the TLP is significantly altered as illustrated in Figure 22 and Figure 23 respectively. Since the mooring lines are now at an angle with the vertical, heave becomes coupled to surge and resonates at the surge frequency. The surge and pitch resonances are barely affected by the wind speed, however sway and roll become coupled to yaw which itself is coupled to surge and pitch through the gyroscopic effect. In this case, all modes of motion are excited even when the waves are aligned with the wind. As the wind speed increases and the mooring lines extend further, the yaw resonance shifts to lower frequencies and the roll resonance shifts to higher frequencies, which corresponds to the "split" between the fore-aft and side-to-side modes discussed in paragraph 3.2.2. Despite their symmetrical location around the tower, we also observe slightly different tension responses for the lines 1 and 3 close to the yaw and roll resonances. This is a remarkable consequence of the simultaneous pitch and roll motions due to the gyroscopic effect; the fact that the rotor spins in one (arbitrary) direction breaks the lateral symmetry of the braces.
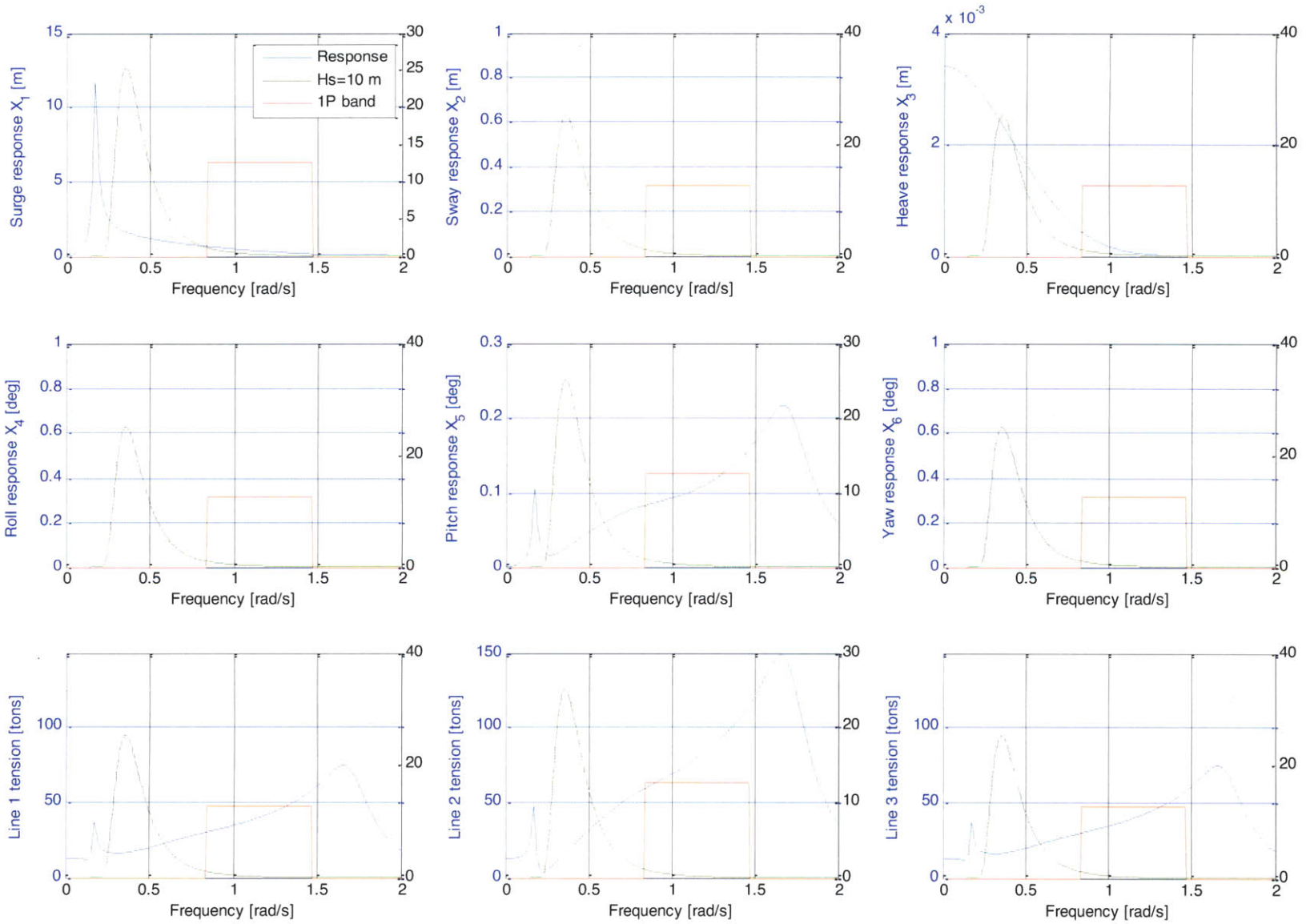
Figure 21: Motion and tension RAOs for a TLP without mean wind
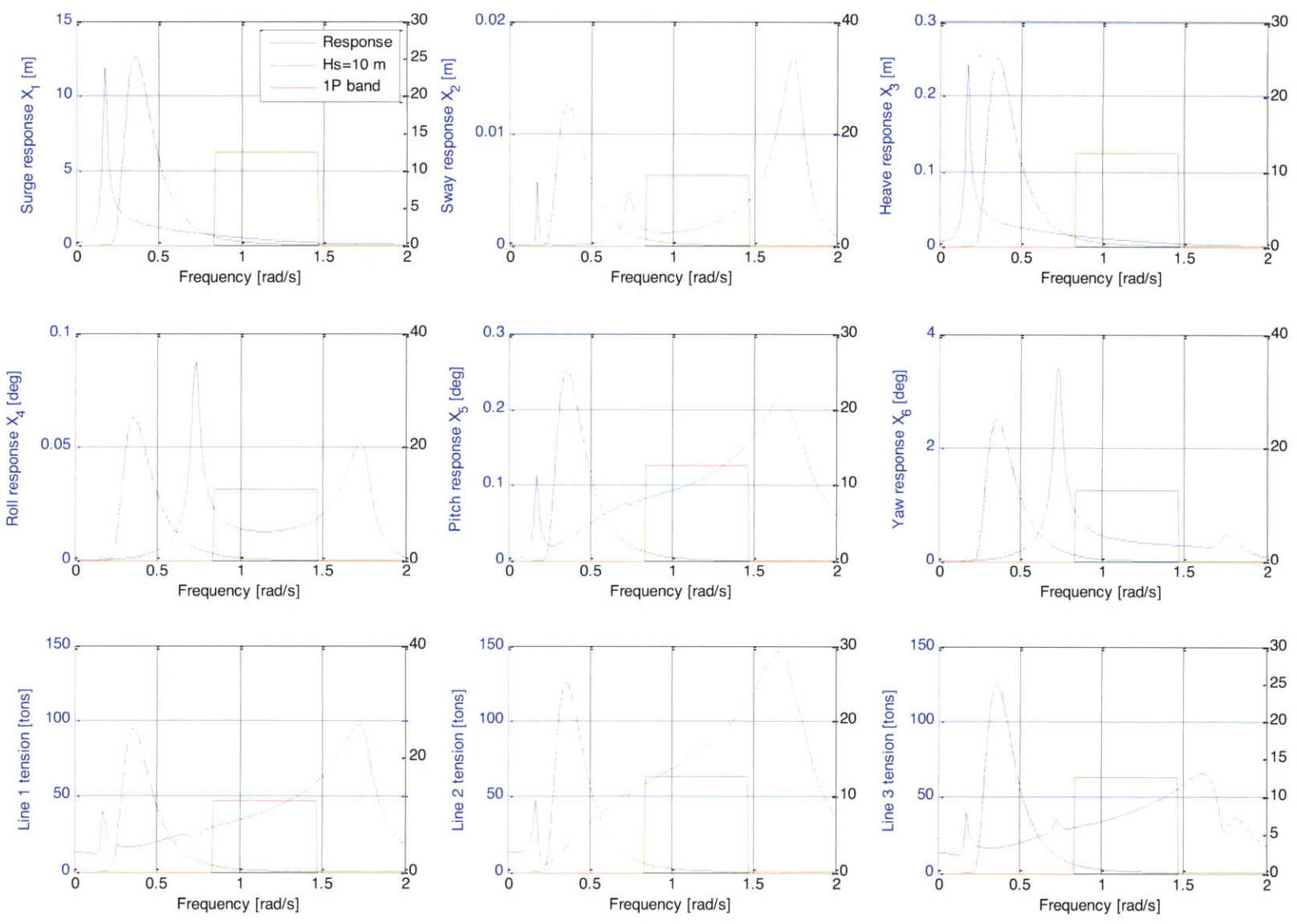
Figure 22: Motion and tension RAOs for a TLP at intermediate wind speed (U=7 m/s)
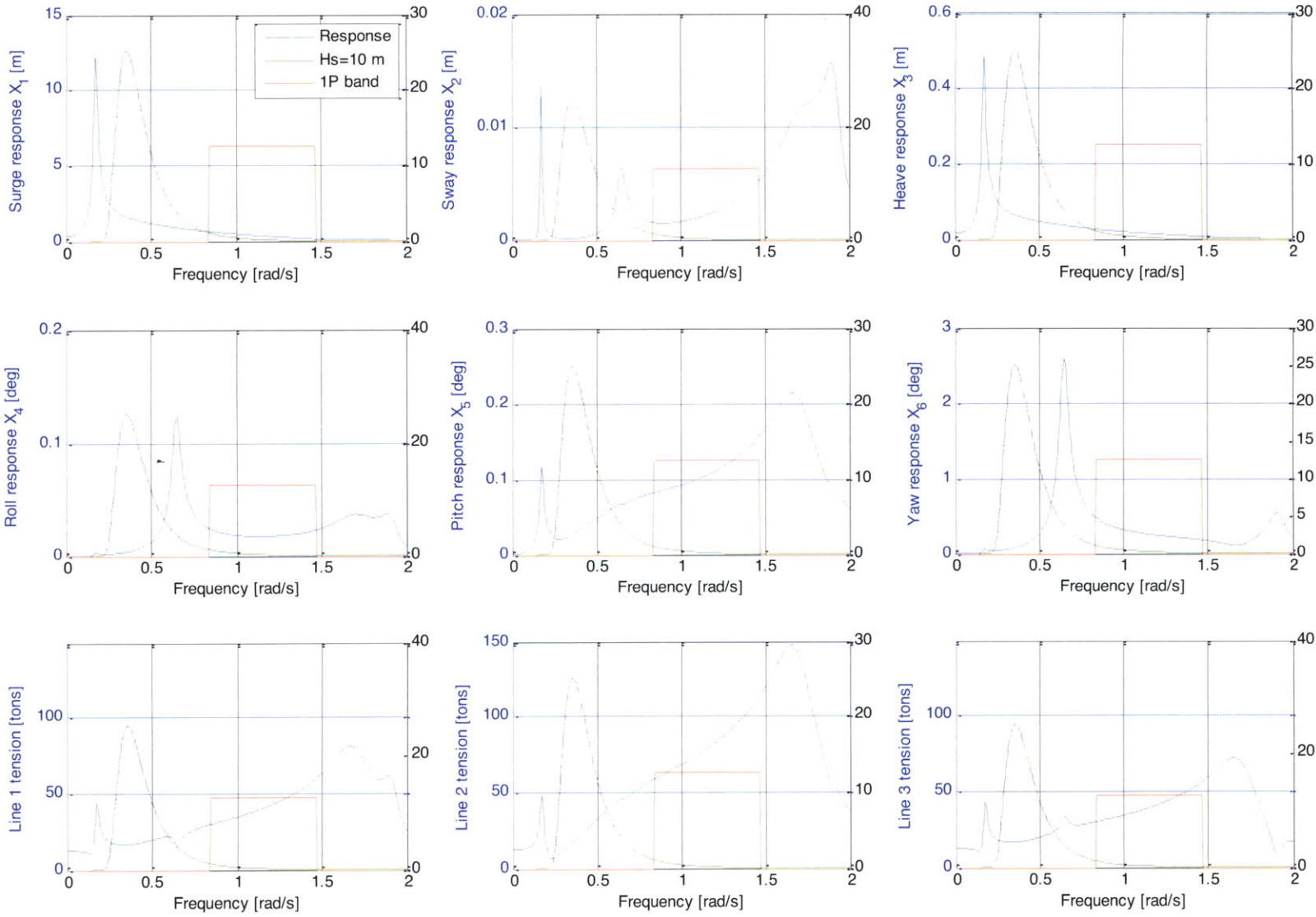
Figure 23: Motion and tension RAOs for a TLP at rated wind speed (U=11 m/s)

58

4.3 Comparison with the rigid TLP

Comparing the rigid and flexible RAOs provides key insights into the structure's behavior and also helps check the validity of Tower Flex. First, the RAOs for the rigid TLP have been calculated in Tower Flex using a very high stiffness ($E \rightarrow \infty$) and compared to the theoretical rigid body RAOs given by Eq. (1.6). The agreement between the two sets of RAOs shown in Figure 24 is excellent and provides a compelling validation of Tower Flex.

The RAOs for the rigid and the flexible structure are then compared in Figure 25 over a broader frequency range [0-3 rad/s] to see the resonance peaks of the rigid structure. The response in surge and heave is virtually identical in the two cases, which confirms that the surge mode is essentially rigid as already observed in Chapter 3. In the case of the flexible TLP, the resonances in pitch and roll occur at lower frequencies where the wave excitations are larger (see paragraph 4.1), therefore the response in these modes is also larger than in the case of the rigid structure. Although the resonance in yaw occurs at the same frequency in both cases, its coupling with pitch also results in larger responses in the case of the flexible structure.
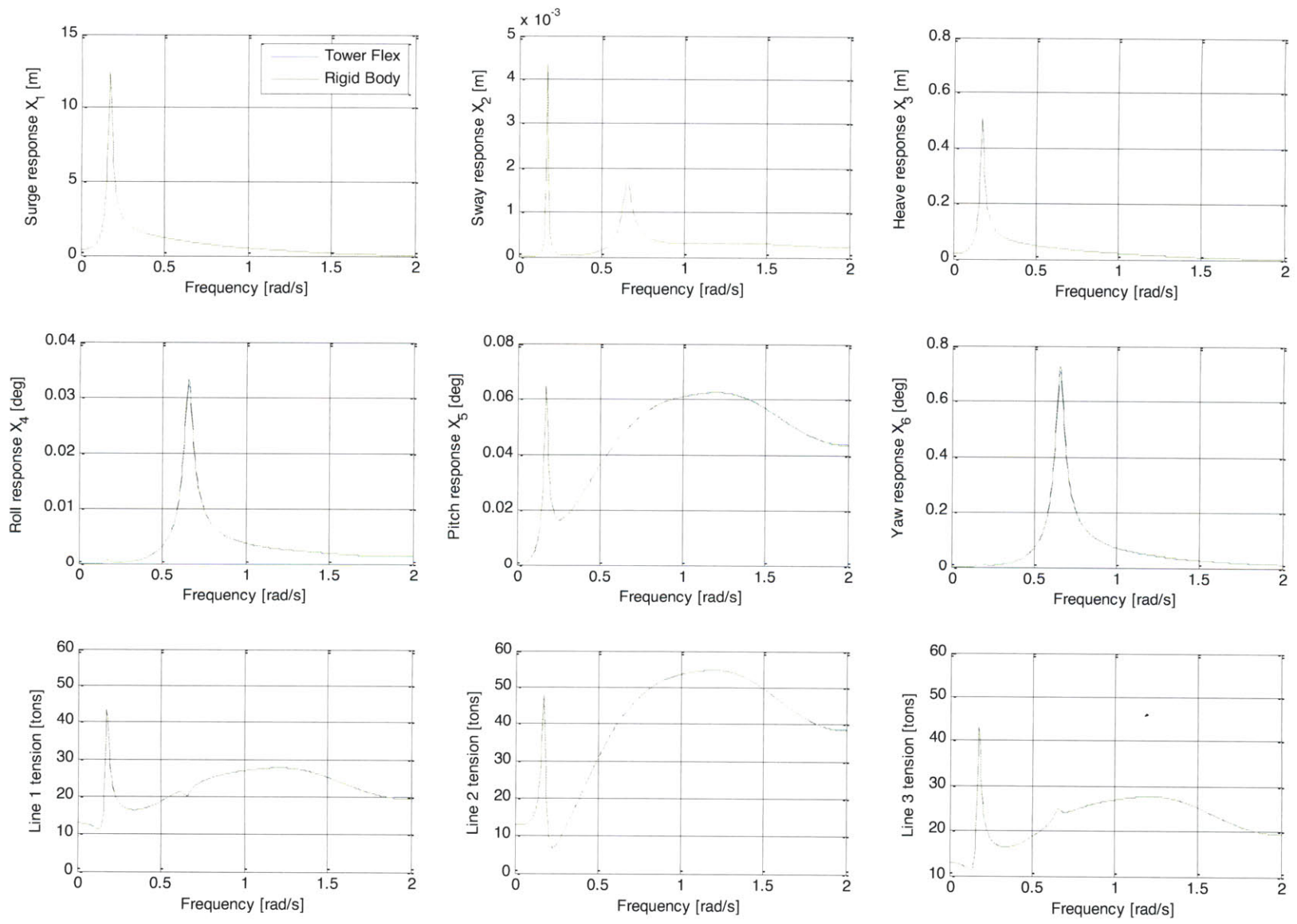
Figure 24: Motion and tension RAOs for the rigid TLP at rated wind speed
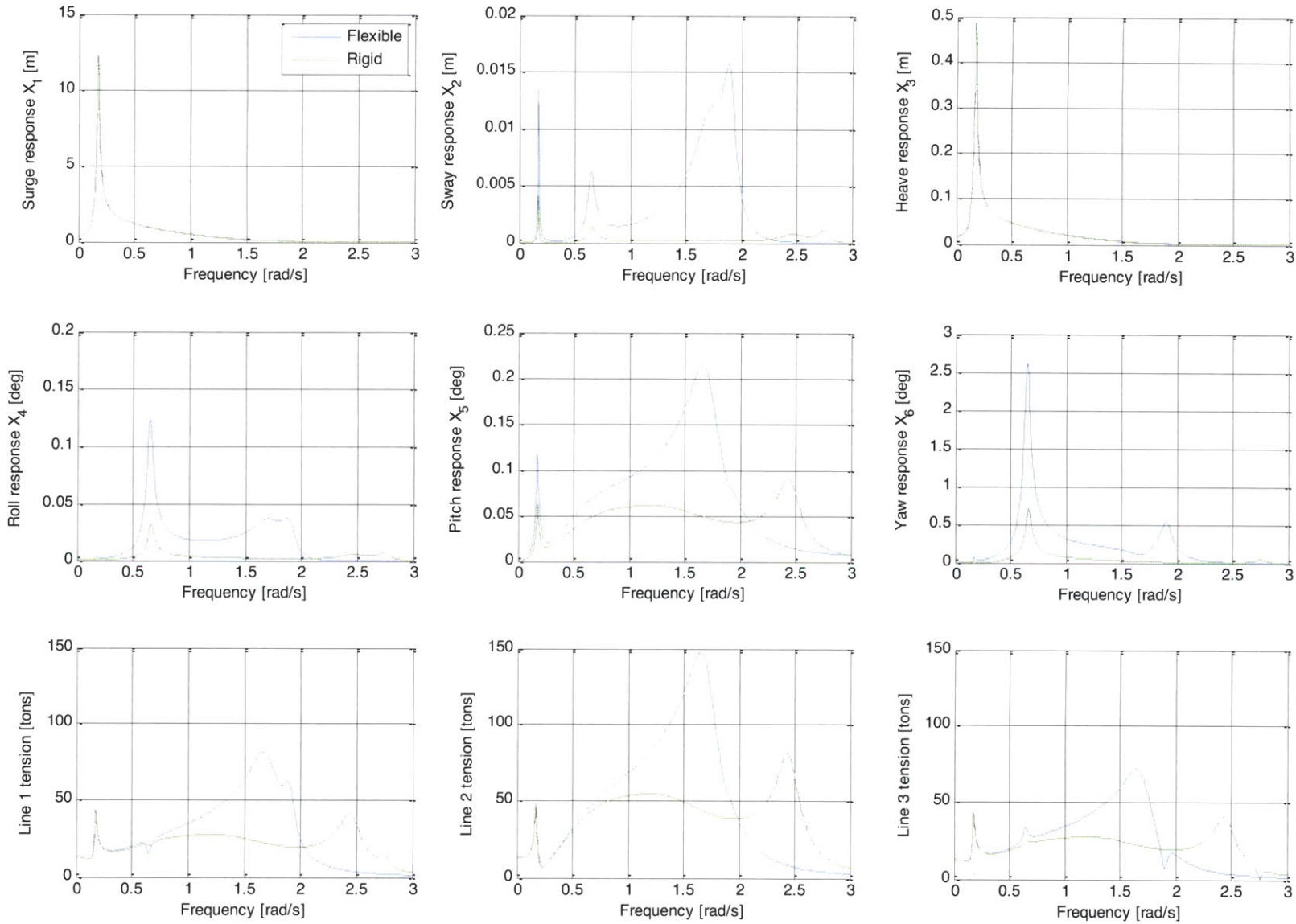
Figure 25: Comparison of the RAOs for the rigid and flexible TLP at rated wind speed

4.4 Motion and tension RMS

Given a Response Amplitude Operator $RAO_i(\omega)$ and the one-sided sea spectrum $S_{wave}(\omega)$, the magnitude of the response can be measured by its standard deviation, or root mean square (RMS), as given by Wiener-Khinchine's theorem [5]

$$\sigma_i^2 = \int_0^\infty |RAO_i(\omega)|^2 S_{wave}(\omega)d\omega \qquad (4.1)$$

The RMS are calculated under a mean wind speed of 11 m/s and in a severe sea state with a significant wave height $H_s = 10$m and a mean spectral period $T_p = 13.6$ s. The corresponding wave spectral density is given by the Pierson-Moskowitz formula as recommended by the ITTC (International Towing Tank Conference)

$$S_{wave}(\omega) = H_s^2 T_p \frac{0.11}{2\pi}\left(\frac{\omega T_p}{2\pi}\right)^{-5} e^{-0.44\left(\frac{\omega T_p}{2\pi}\right)^{-4}} \qquad (4.2)$$

Dynamic properties	Rigid	Flexible	Relative difference
Surge RMS [m]	3.69	3.68	-0.2%
Sway RMS [m]	0.001	0.004	421%
Heave RMS [m]	0.15	0.15	0.5%
Roll RMS [deg]	0.02	0.07	307%
Pitch RMS [deg]	0.08	0.12	42.5%
Yaw RMS [deg]	0.37	1.42	280%
Nacelle acceleration RMS [g]	0.08	0.09	8.3%
Line 1 tension RMS [tons]	46	50	13.0%
Line 2 tension RMS [tons]	69	77	11.0%
Line 3 tension RMS [tons]	47	52	17.1%
Line 1 static -2σ dynamic tension [tons]	20	12	-38.3%
Line 2 static -2σ dynamic tension [tons]	118	101	-15.1%
Line 3 static -2σ dynamic tension [tons]	19	9	-54.0%
Line 1 static +2σ dynamic tension [tons]	204	212	3.7%
Line 2 static +2σ dynamic tension [tons]	392	410	4.5%
Line 3 static +2σ dynamic tension [tons]	205	216	5.0%

Table 13: Dynamic properties of the TLP at rated wind speed (U=11 m/s) and Hs=10m

The results listed in Table 13 above show that except for surge, the TLP undergoes very small displacements in all modes of motion. The non-zero roll motion causes a small discrepancy between the tension RMS of lines 1 and 3; however the condition for these leeward lines not to go slack ($[T_{pre} - T_{static} - 2\sigma_{Tdyn}] > 0$) is still satisfied. The results also highlight the larger sway, roll and yaw motions of the flexible structure compared to its rigid equivalent.

5 Fatigue analysis

Fatigue is the process by which the repeated application of loads and the associated stress cycles create cracks and cause the structure to fail. Fatigue is the primary design driver for wind turbines, and is particularly critical in the case of offshore wind turbines which are subject to simultaneous wind and wave loads.

5.1 Methodology

5.1.1 Hot spots

The fatigue analysis is conducted at the critical locations ("hot spots") of the structure shown in Figure 26:
- at the tower base where the bending moment from the wind thrust is maximum
- at the brace roots

5.1.2 Design load cases

The design load cases (DLCs) for fatigue are described in the IEC 61400-3 norm for offshore wind turbines [14] and summarized below:

- **1.2 (Normal Power Production)**
- 2.4 (Power Production+fault)
- 3.1 (Start-up)
- 4.1 (Normal shutdown)
- 6.4 (Parked)
- 7.2 (Parked+fault)
- 8.3 (Transport)

In this work, we shall focus on the DLC 1.2 (Normal Power Production) which is expected to be the most frequent DLC over the turbine's lifetime and therefore the main contributor to fatigue damage.
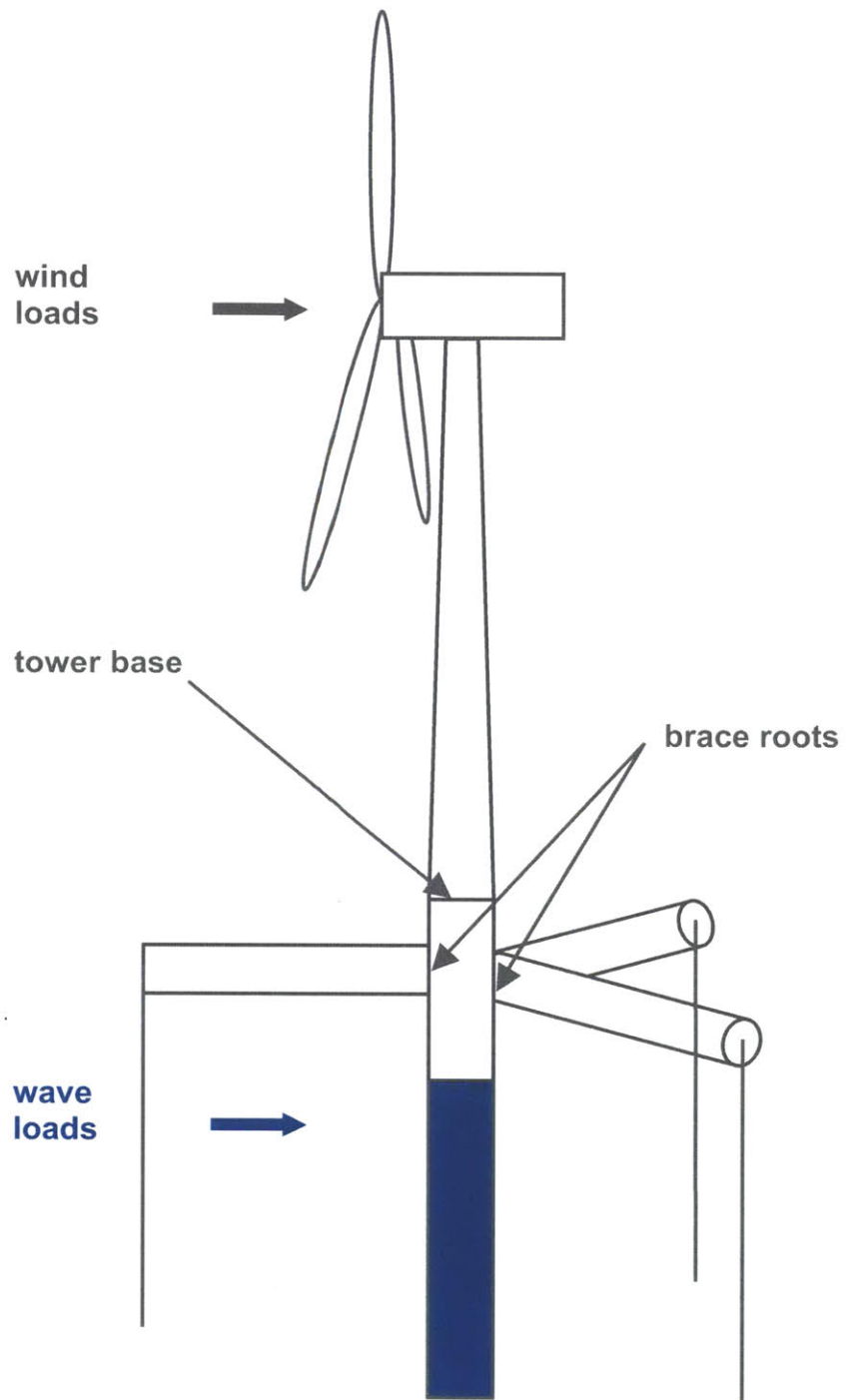
Figure 26: Location of the hot spots for the fatigue analysis

5.1.3 Input spectra for the frequency-domain analysis

Fatigue is analyzed in the frequency domain using excitation spectra for the wind and wave loads and following the recommendations of the IEC norm [14].

For the wind loads, we have obtained time records of the forces and moments at the hub shown in various operating conditions including the DLC 1. Figure 27 shows the conventions used for these loads at the hub level. Time series are available for 12 different mean wind speeds between cut-in (3 m/s) and cut-out speeds (25 m/s), and each one of them represents a record of 600s (10min) at a sampling rate of 20 Hz.
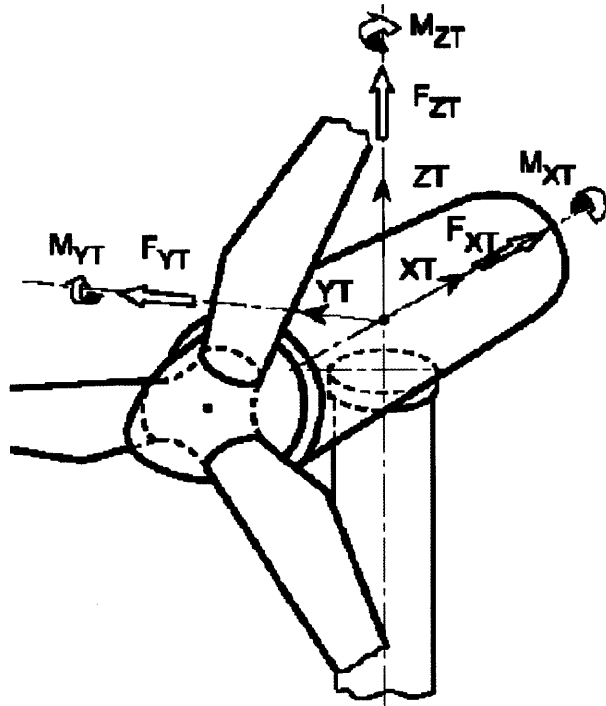
Figure 27: Definition of the wind loads at the hub

The main source of dynamic loads on the turbine comes from the thrust Fx. The transverse Fy component is essentially equal to zero and can be neglected for fatigue purposes. Similarly, the vertical component Fz is essentially static (due to gravity) and does not induce any significant load cycles. The Mx moment is the rotor torque that is transmitted to the generator and can therefore be disregarded here. Other sources of dynamic loads are the tilt moment My which contributes to the bending moment on the tower and the yaw moment Mz which induces pitch motion through gyroscopic effects.

Given these observations, the thrust, tilt moment and yaw moment PSDs been computed using Welch's method on the detrended signal (subtracting its mean value). The frequency step (resolution) is $10/8192=0.0012$ Hz and the Nyquist frequency is 10 Hz (half the sampling frequency of 20 Hz). A key observation is that most of the energy content of the wind is in the low frequency range (below 1 Hz).

For the wave loads, each wind speed U is related to a significant wave height $E[H_s|U]$ and median peak spectral period T_p according to the joint probability of metocean parameters described in [19]. The corresponding wave spectral density is given by the Pierson-Moskowitz formula, where the 2π factor is dropped when Hz are used vs. rad/s

$$S_{\text{wave}}(f) = 0.11 H_s^2 f^{-5} T_p^4 \, e^{-0.44(fT_p)^{-4}} \tag{5.1}$$

Table 14 summarizes the wind and wave conditions used for fatigue assessment. Note that the wind speed distribution is given by a Weibull distribution

$$f(U) = \frac{k}{C}\left(\frac{U}{C}\right)^{k-1} e^{-\left(\frac{U}{C}\right)^k} \tag{5.2}$$

with

$$C = \frac{U_{avg}}{\Gamma(1+1/k)} \tag{5.3}$$

In the present case, the Weibull distribution plotted in Figure 28 has a shape factor $k=2$ (it is identical to a Rayleigh distribution) and a long term average wind speed $U_{avg} = 8.5$ m/s.
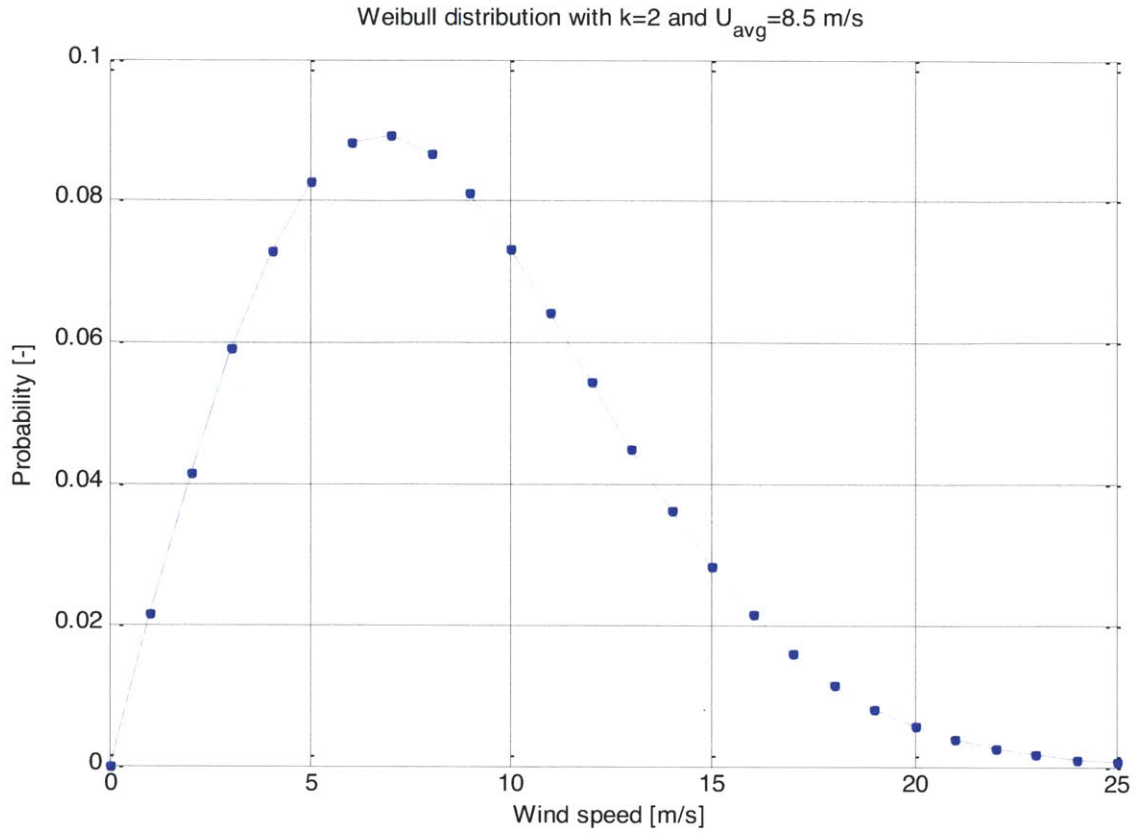
Figure 28: Weibull distribution of wind speed

Wind speed U (m/s)	Bin lower limit (m/s)	Bin upper limit (m/s)	$E[H_s\|U]$ (m)	T_p (s)	Weibull probability (k=2, Uavg=8.5 m/s)
3	2	4	2.0	9.7	11.71%
5	4	6	2.3	9.8	16.42%
7	6	8	2.8	9.9	17.75%
9	8	10	3.2	10.1	16.15%
11	10	12	3.8	10.4	12.82%
13	12	14	4.3	10.6	9.02%
15	14	16	4.9	10.9	5.69%
17	16	18	5.5	11.1	3.23%
19	18	20	6.1	11.4	1.66%
21	20	22	6.8	11.7	0.77%
23	22	24	7.5	12.0	0.33%
25	24	25	8.2	12.3	0.08%

Table 14: Joint wind/wave conditions used for fatigue assessment

Finally, while different orientations of the incident waves relative to the wind can be taken into account, we have focused on the most conservative case where wind and waves are co-directional. This choice is consistent with guidelines provided by the IEC [14] and with previous fatigue studies [8,10,11].

5.1.4 Calculation of stress PSDs

Fatigue assessment is based on the nominal bending stresses, which are calculated at different angles θ around the analyzed cross-section as follows

$$\sigma = \frac{-F_5 R \cos\theta + F_4 R \sin\theta}{I} \tag{5.4}$$

for the tower and

$$\sigma = -\frac{M_z R \cos\theta}{I_{zz}} + \frac{M_y R \sin\theta}{I_{yy}} \tag{5.5}$$

for the braces.

The stress transfer function for a unit wave amplitude is obtained by linear summation of the individual stress transfer functions

$$H_\sigma(f,\theta) = \sum_i H_{\sigma_i}(f,\theta) F_i^{\text{HYDRO}}(f) \tag{5.6}$$

where

$H_{\sigma_i}(f,\theta)$ is the stress transfer function for a unit load in direction i at different angles θ around the analyzed cross-section

F_i^{HYDRO} is the wave excitation in direction i for a unit wave amplitude

The PSD of the wave loads is then obtained by applying Wiener-Khinchine's theorem

$$S_{\sigma_{\text{wave}}}(f,\theta) = \left|H_\sigma(f,\theta)\right|^2 S_{\text{wave}}(f) \tag{5.7}$$

For the wind loads, the thrust, tilt moment and yaw moment are assumed to be uncorrelated so that the total stress PSD is the sum of the stress PSDs obtained for each individual excitation

$$S_{\sigma_{\text{wind}}}(f,\theta) = \sum_i \left| H_{\sigma_i}(f,\theta) \right|^2 S_{i\,\text{wind}}(f) \qquad (5.8)$$

where

$H_{\sigma_i}(f,\theta)$ is the stress transfer function for a unit load in direction i at different angles θ around the analyzed cross-section

$S_{i\,\text{wind}}$ is the PSD of the wind excitation in direction i

5.1.5 Truncation of stress peaks

For the computation of the stress transfer functions, an equivalent structural damping is implemented by truncating the stress peaks to obtain a 2% damping ratio using the half-bandwidth method [4].
Figure **29** provides an illustration of this method in the case of the surge force to stress transfer function on the tower base.
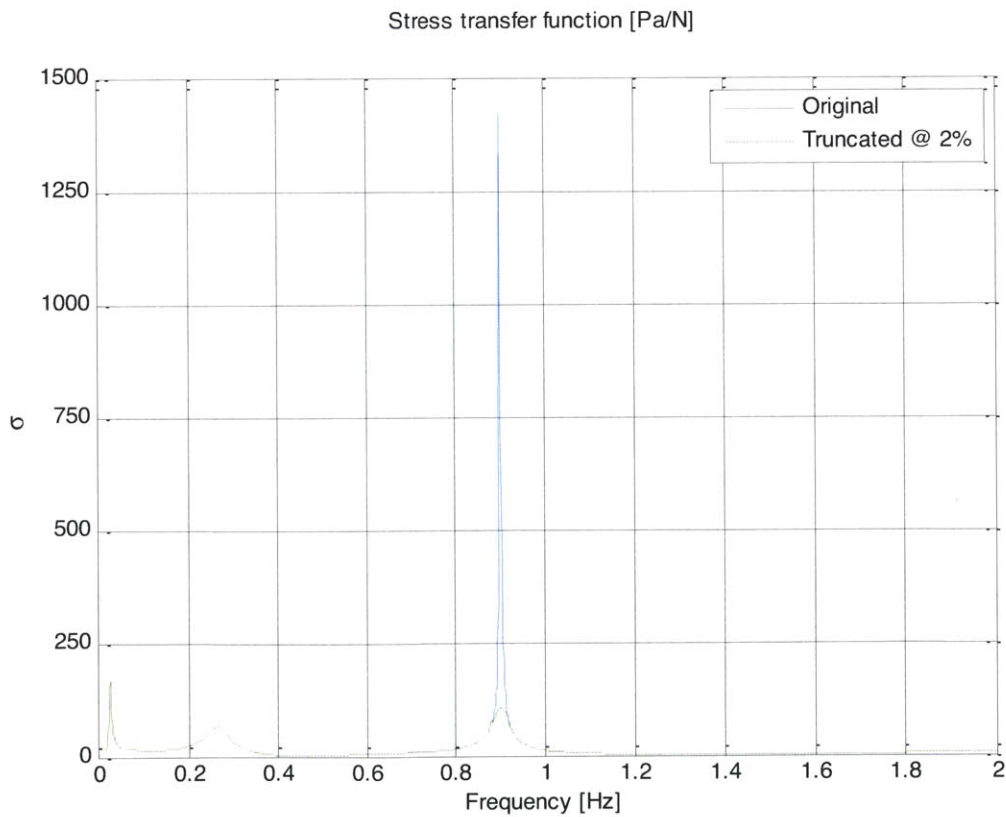
Figure 29: Original and truncated stress transfer function

70

5.1.6 Post-processing: calculation of fatigue damage and lifetime

If the excitation signal from the wind or the waves can be assumed to be Gaussian then the response will also be Gaussian. Let us suppose that the S-N curve is given by the relationship

$$N\sigma^m = C \tag{5.9}$$

where σ is the nominal stress amplitude (equal to half the stress range) and m is the "slope"[†]. If damage is accumulated linearly according to Miner's rule, the total expected damage over time T is [13]

$$E[D] = \frac{n_p^+ T}{C} \int_0^{+\infty} \sigma^m q(\sigma) d\sigma \tag{5.10}$$

where n_p^+ is the number of maxima per unit time and $q(\sigma)$ the probability distribution of stress peaks. These quantities are the frequency-domain equivalents of the number of cycles and the amplitude of cycles in the time domain.

For a Gaussian process, $q(\sigma)$ distribution is a weighted sum of Rayleigh and Gaussian distributions that depends on the irregularity factor $r = n_0^+ / n_p^+$, ratio of the expected frequency to the mean number of maxima per second ($0 \leq r \leq 1$)

$$q(u = \sigma / \sigma_{\mathrm{RMS}}) = \sqrt{\frac{1-r^2}{2\pi}} e^{-\frac{u^2}{2(1-r^2)}} + \frac{ur}{2} e^{-\frac{u^2}{2}} \left[1 + \mathrm{erf}\left(\frac{ur}{2(1-r^2)} \right) \right] \tag{5.11}$$

σ_{RMS}, n_0^+, n_p^+ and r can be calculated from the stress PSD $S_\sigma(f,\theta)$ as follows

$$\begin{aligned}
\sigma_{RMS} &= \sqrt{m_0} \\
n_0^+ &= \sqrt{m_2 / m_0} \\
n_p^+ &= \sqrt{m_4 / m_2} \\
r &= n_0^+ / n_p^+ = m_2 / \sqrt{m_0 m_4}
\end{aligned} \tag{5.12}$$

where $m_n = \int_0^{+\infty} S_\sigma(f,\theta) f^n \, df$ is the n-th moment of the stress PSD (theory of S.O. Rice).

[†] The actual slope of the S-N curve in logarithmic scales is $-1/m$

Formulas for the expected damage over time T are shown in Table 15 below:

Type of response	Probability distribution of the stress peaks	Expected Damage over time T
Narrow-band (r~1)	Rayleigh	$E[D] = \dfrac{n_p^+ T}{C}(\sqrt{2}\sigma_{\mathrm{RMS}})^m \Gamma\left(1+\dfrac{m}{2}\right)$ ‡
Intermediate	Weighted sum of Rayleigh and Gaussian	$E[D] = \dfrac{n_p^+ T}{C}\sigma_{\mathrm{RMS}}^m \displaystyle\int_0^{+\infty} u^m q(u)\,du$
Wide-band (r~0)	Gaussian	$E[D] = \dfrac{n_p^+ T}{2C\sqrt{\pi}}(\sqrt{2}\sigma_{\mathrm{RMS}})^m \Gamma\left(\dfrac{m+1}{2}\right)$

Table 15: Expected fatigue damage for different types of responses

It should be noted that the narrow-band response corresponds to that of a lightly damped 1-DOF system, and that the associated Rayleigh distribution for the stress peaks results in the highest value for the damage (conservative case).

Once the expected yearly damage has been calculated, the expected fatigue life T is obtained by equating the damage to unity, yielding

$$T = 1/D \qquad\qquad (5.13)$$

5.1.7 Choice of S-N curve

The S-N curve has been chosen according to the DNV rules [16] (or equivalently, the IIW rules [18]) for a welded hollow cross-section made of steel. It is described as follows

$$\begin{cases} N\sigma^{m_1} = N_R\sigma_R^{m_1} = C_1 & \text{for } N \leq 10^7 \\ N\sigma^{m_2} = N_K\sigma_K^{m_2} = C_2 & \text{for } N \geq 10^7 \end{cases} \qquad (5.14)$$

The parameters in (5.14) are summarized in Table 16 and illustrated in Figure 30 below, where the stress range $\Delta\sigma = 2\sigma$ is considered instead of stress amplitude σ.

---

*‡ Often n_0^+ is used instead of n_p^+, which does not matter if r~1. However if r is different from 1, replacing n_0^+ by n_p^+ is justified since the damage is related to the number of peaks [13].
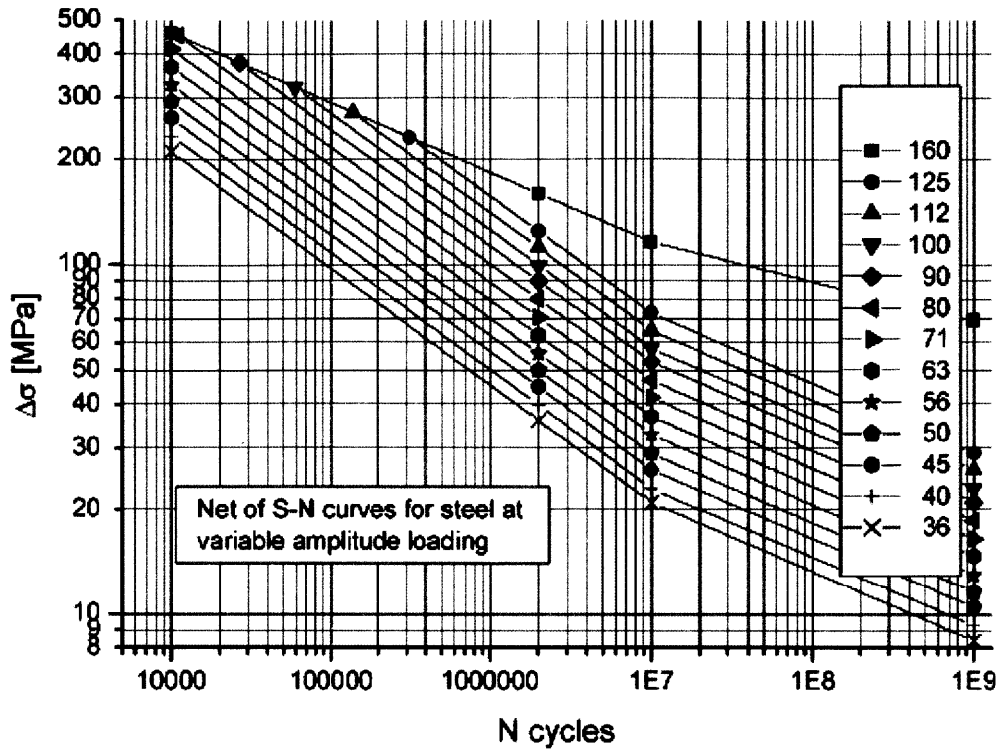
Figure 30: S-N curve of welded steel used in fatigue calculations [18]

The S-N curve in Figure 30 varies across two different regions separated by the so-called "knee point". The first region on the left corresponds to a low number of cycles with a slope equal to 3; the second one corresponds to a high number of cycles with a slope equal to 5. To be conservative, we do not consider any constant amplitude fatigue limit - below which failure does not occur - as it is believed that low but variable stresses do contribute to fatigue damage [18].

$N \leq 10^7$	N_R (reference number of cycles)	2.10^6
	σ_R (reference fatigue strength) [MPa]	80/2=40
	Fatigue exponent m_1	3
$N \geq 10^7$	N_K (number of cycles at the knee point)	10^7
	$\sigma_K = \sigma_R (N_R / N_K)^{1/m_1}$ (fatigue strength at the knee point) [MPa]	23
	Fatigue exponent m_2	5

Table 16: Parameters of the two-slope S-N curve of steel used in fatigue calculations

In practice, we have analyzed three cases:
- a single-slope curve with m=3 that extends to the high-cycle region
- a single-slope curve with m=5 that extends to the low-cycle region
- a two-slope curve as shown in Figure 30

For the latter case, the damage has been calculated assuming a Rayleigh distribution of the stress peaks [16]

$$E[D] = n_p^+ T \left[\frac{\left(\sqrt{2}\sigma_{RMS}\right)^{m_1}}{C_1} \left(1 - \gamma\left(1 + \frac{m_1}{2}, \frac{\sigma_K^2}{2\sigma_{RMS}^2}\right)\right) + \frac{\left(\sqrt{2}\sigma_{RMS}\right)^{m_2}}{C_2} \gamma\left(1 + \frac{m_2}{2}, \frac{\sigma_K^2}{2\sigma_{RMS}^2}\right) \right] \quad (5.15)$$

where γ is the incomplete gamma function.

5.1.8 Other assumptions

- Choice of frequency range: the stress PSD have been calculated
  - between 0 and 3 rad/s for the wave loads
  - between 0 and 10 Hz for the wind loads

- No mean stress effects have been accounted for in fatigue calculations

- No stress concentration factors other than those included in the chosen S-N curve have been used in load calculations

- No partial safety factors have been used in calculating the loads or the fatigue strength

- Given the relatively high location of the tower base and of the braces relative to the sea level, the effect of seawater on the S-N curve has not been taken into account

5.2 Results

For each wind speed listed in Table 14, the stress PSDs have been calculated at different locations around the cross-sections. The maximum damage has been found to occur at 0/180 degrees for the tower base (corresponding to the fore-aft bending of the tower) and at +/- 90 degrees for the braces (corresponding to the vertical bending of the braces).

74

5.2.1 Wave loading

Figure 31 shows, for each of the critical locations, the stress transfer function for a unit wave amplitude, the sea spectrum at rated wind speed and the resulting stress power spectral density (PSD). Not surprisingly, the stress transfer functions are similar in shape to the motion RAOs shown in Figure 23.
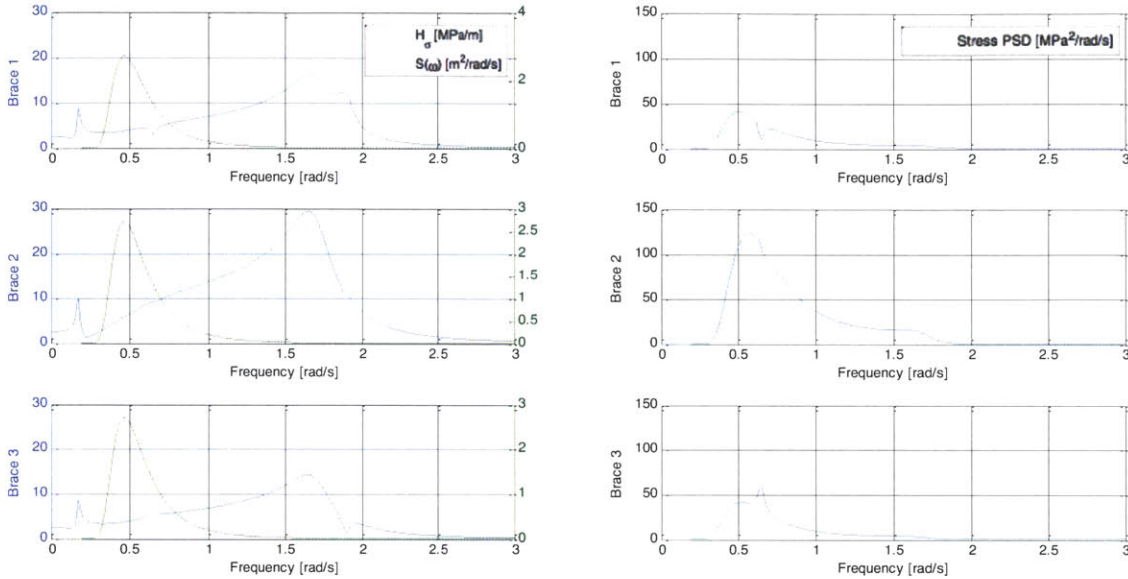
Figure 31: Stress transfer function and PSD for the wave loading at rated wind speed

Table 17 presents the statistics of the stress PSDs obtained at different wind speeds and weighted by the probabilities listed in Table 14. The mean number of peaks per second is about 0.2, which amounts to about 5 million cycles per year or 10^8 cycles over 20 years.

Table 18 presents the expected fatigue life of the different components according to the type of response and the slope of the S-N curve. As expected, a Rayleigh distribution of the stress peaks yields in the largest damage and the shortest fatigue life. On the other hand, a Gaussian distribution will result in the longest fatigue life. Regardless of the nature of the distribution of the stress peaks, it appears that the tower base as well as the second (windward) brace are the most prone to failure over 20 years. It is clear that the tower, which has been designed for an onshore machine, is not suited to an offshore environment.

The influence of the slope on fatigue life depends on the amplitude of the stress cycles compared to the reference strength at the knee point. Except for the tower, the stress RMS is much smaller than the fatigue strength at the knee point therefore most of the damage is due to a high number of low amplitude cycles, where a slope $m=5$ yields a

longer fatigue life. This is confirmed by looking at the case of the two-slope S-N curve, for which results are almost identical to those of the m=5 case.

Location	σ_{RMS} [MPa]	n_0^+ [Hz]	n_p^+ [Hz]	r factor
Tower base	15.5	0.14	0.19	0.75
Brace root 1	4.4	0.14	0.19	0.71
Brace root 2	8.1	0.14	0.19	0.75
Brace root 3	4.7	0.13	0.18	0.73

Table 17: Statistics of the stress distribution due to the wave loading

		Lifetime (years)		
		Rayleigh	Intermediate	Gaussian
Tower	m=3	2	2	7
	m=5	1	1	4
	two-slope	2	-	-
Brace root 1	m=3	65	90	305
	m=5	363	510	2,136
	two-slope	363	-	-
Brace root 2	m=3	11	14	52
	m=5	18	24	108
	two-slope	20	-	-
Brace root 3	m=3	60	81	281
	m=5	297	407	1,749
	two-slope	297	-	-

Table 18: Fatigue life due to the wave loading

5.2.2 Wind loading

Figure 32 shows, for each of the critical locations, the stress transfer function for a unit thrust, the thrust spectrum at rated wind speed and the resulting stress power spectral density (PSD).

Table 19 presents the statistics of the stress PSDs obtained at different wind speeds and weighted by the probabilities listed in Table 14. The maximum number of peaks per second is about 0.4, which amounts to about 10 million cycles per year or 2.10^8 cycles over 20 years.

Table 20 presents the expected fatigue life of the different components according to the type of response and the slope of the S-N curve. The tower base is still the most critical location, while all the brace roots have comparable lifetimes well over 20 years in the case of a two-slope curve. Compared to the wind loading, the amplitude of the stress cycles (measured by σ_{RMS}) is smaller; however the number of cycles (measured by n_0^+ or n_p^+) is much higher due to the high frequency components of the wind loads.
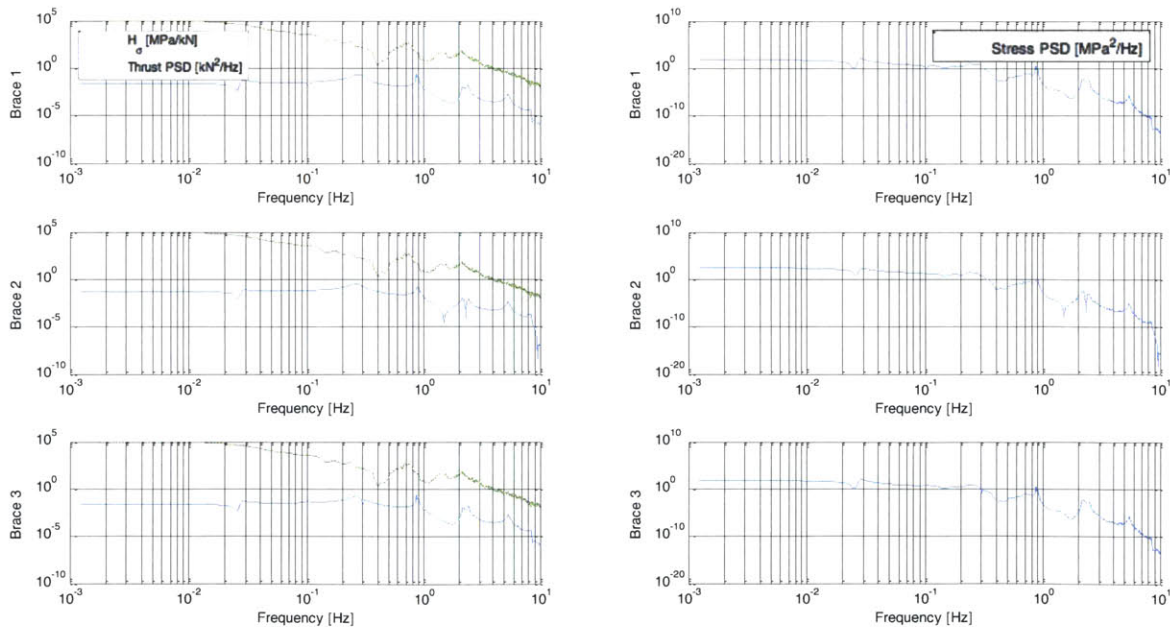

Figure 32: Stress transfer function and PSD of the thrust at rated wind speed

Location	σ_{RMS} [MPa]	n_0^+ [Hz]	n_p^+ [Hz]	r factor
Tower base	8.3	0.18	0.39	2.05
Brace root 1	3.7	0.24	0.28	1.13
Brace root 2	3.7	0.30	0.31	0.95
Brace root 3	3.7	0.23	0.27	1.16

Table 19: Statistics of the stress distribution due to the wind loading

		Lifetime (years)		
		Rayleigh	Intermediate	Gaussian
Tower	m=3	1	3	4
	m=5	1	5	8
	two-slope	1	-	-
Brace root 1	m=3	19	52	88
	m=5	145	460	855
	two-slope	145	-	-
Brace root 2	m=3	23	56	109
	m=5	172	483	1,012
	two-slope	172	-	-
Brace root 3	m=3	19	54	89
	m=5	150	490	881
	two-slope	150	-	-

Table 20: Fatigue life due to the wind loading

In the case of the wind loading it is interesting to understand the respective contribution to fatigue of the different loads (thrust, tilt and yaw) to fatigue. Figure 33 shows the breakdown of the total stress RMS into its various components, which are assumed to be independent such that

$$\sigma^2_{RMS} = \sigma^2_{THRUST} + \sigma^2_{TILT} + \sigma^2_{YAW} \tag{5.16}$$
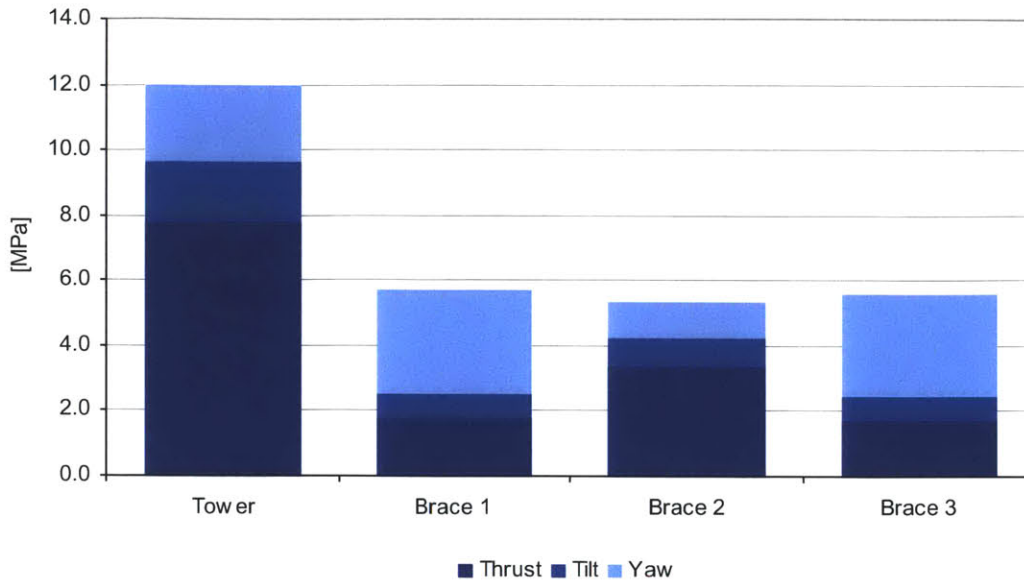
Figure 33: Breakdown of the stress RMS for to the wind loading

Not surprisingly, the thrust (or more accurately, the fluctuations of the thrust around its mean value) accounts for most of the stress level on the tower base and the windward brace. For the two lateral braces however, it is yaw (and the resulting rolling motion) that contributes the most to the stress level.

5.3 Sensitivity analysis

Fatigue is a complex topic that relies on many assumptions regarding the calculation of stresses and the subsequent damage incurred by the structure. The lifetimes presented in this work should be considered carefully and depend on a number of parameters. In this section, we analyze the sensitivity of fatigue life to the following parameters: the structural damping ratio and the cut-off frequency.

Sensitivity to the structural damping ratio

We have analyzed the impact of different structural damping ratios (1%, 2% and 3%) on the fatigue life of the proposed design. Results for the wind loading are presented in Table 21 and illustrated in Figure 34. They confirm the intuition that a higher value of the structural damping increases fatigue life. However, this effect is relatively small for wind and non-existent for the low-frequency wave excitations, which is consistent with previous observations [12].

| | Structural damping | | |
Location	1%	2% (base case)	3%
Tower base	1	1	2
Brace root 1	118	145	162
Brace root 2	145	172	198
Brace root 3	121	150	165

<p align="center">Table 21: Fatigue life (in years, assuming Rayleigh distribution) due to the wind loading</p>
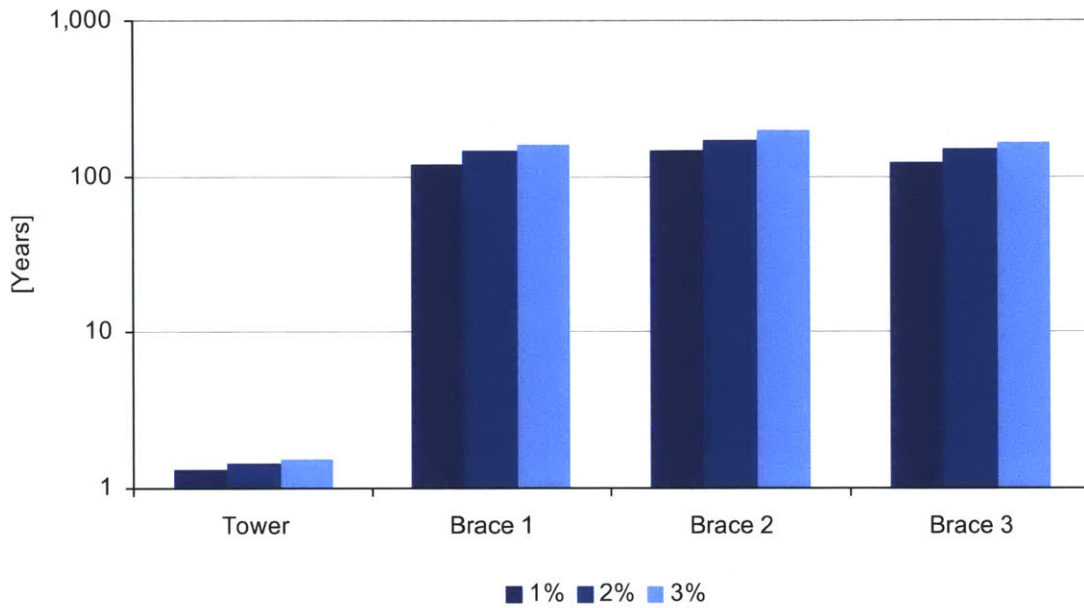
<p align="center">Figure 34: Fatigue life due to wind loading as a function of the structural damping ratio</p>

Sensitivity to the cut-off frequency

Although the wind contains little energy at high frequencies, the cut-off frequency can significantly affect the fatigue life since high frequency tower modes can still be excited. We have run the fatigue analysis using different cut-off frequencies (0.1, 1 and 5 Hz) for the wind loading. Results compiled in Table 22 to Table 24 and plotted in Figure 35. Despite a marginally higher stress RMS, a higher cut-off frequency results in a larger number of cycles and a larger damage. Fortunately there is little difference between the results obtained for 5 Hz and 10 Hz, therefore we can assume that results have converged at 10 Hz.

Location	σ_{RMS} [MPa]	n_0^+ [Hz]	n_p^+ [Hz]	r factor	Lifetime [years] - Rayleigh
Tower base	7.1	0.46	0.03	0.07	100
Brace root 1	2.1	0.77	0.07	0.09	33,491
Brace root 2	2.9	0.54	0.04	0.07	9,168
Brace root 3	2.1	0.77	0.07	0.09	32,879

Table 22: Fatigue life due to the wind loading (cut-off=0.1 Hz)

Location	σ_{RMS} [MPa]	n_0^+ [Hz]	n_p^+ [Hz]	r factor	Lifetime [years] - Rayleigh
Tower base	8.3	0.28	0.22	0.78	4
Brace root 1	3.7	0.34	0.26	0.77	218
Brace root 2	3.7	0.38	0.30	0.79	227
Brace root 3	3.7	0.32	0.25	0.77	232

Table 23: Fatigue life due to the wind loading (cut-off=1 Hz)

Location	σ_{RMS} [MPa]	n_0^+ [Hz]	n_p^+ [Hz]	r factor	Lifetime [years] - Rayleigh
Tower base	8.3	0.19	0.39	2.05	2
Brace root 1	3.7	0.25	0.28	1.13	148
Brace root 2	3.7	0.33	0.31	0.95	189
Brace root 3	3.7	0.23	0.27	1.16	153

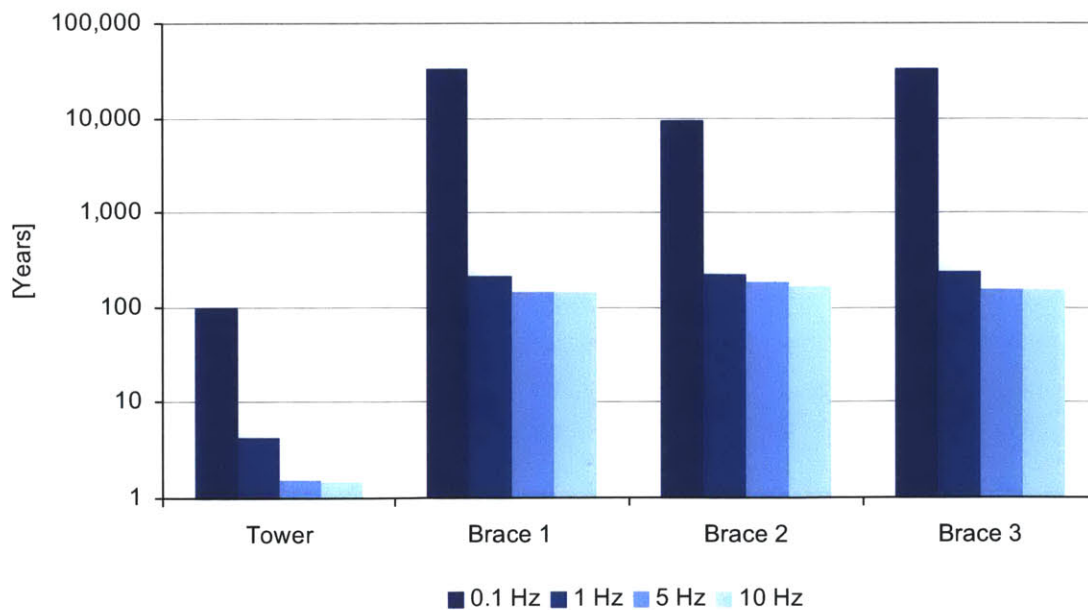Table 24: Fatigue life due to the wind loading (cut-off=5 Hz)

Figure 35: Fatigue life due to the wind loading as a function of the cut-off frequency

5.4 Conclusions

Making use of real-world data and reasonable assumptions, we have estimated the fatigue life due to wind and waves of some of the critical components of the TLP. As currently designed the tower base will most likely fail within 20 years and needs to be reinforced if it is to be part of an offshore structure. On the other hand, the braces have a more conservative design and are expected to last over 50 years in the wind and wave conditions considered in this work.

The sensitivity analyses have highlighted the dependence of fatigue damage on the S-N curve parameters as well as on the cut-off frequency which needs to be large enough to capture high-frequency fatigue loads. On the other hand the value of structural damping – as long as it is non-zero – seems to have little influence on fatigue life.

In a more detailed fatigue analysis, other operational DLCs with yaw or wind/wave misalignment and non-operational DLCs should be considered to comply with the IEC norm [14]. Other structural elements that fall out of the scope of this work (the blade roots, the yaw bearing, the shaft and the mooring lines themselves) should also be investigated. Non-linear, high-frequency springing and ringing wave loads could also be included in order to get a fully comprehensive picture of fatigue damage.

Finally, some remarks apply specifically to our fatigue analysis in the frequency domain. The only way the correlations between the wind and the waves have been taken into account so far has been through the joint probability distribution of the mean wind speed and the significant wave height. Using a quasi-static mean thrust and wind/wave loads spectra weighted by a Weibull distribution, we have been able to calculate the expected damage due to the waves and wind *separately*. Ideally, actual phase correlations between the dynamic wind and wave excitations should be taken into account to properly understand the effect of these simultaneous loads. Alternatively, one could use the combined spectrum or the dual narrow-band approach explained in [17].

6 Conclusion

We have successfully extended a two-dimensional beam model into Tower Flex, a coupled structural dynamics model used for the evaluation of three-dimensional, multibody structures in the frequency domain.

Tower Flex has been used to evaluate a 3MW floating wind turbine mounted on a Tension Leg Platform (TLP). Natural frequencies and Response Amplitude Operators (RAOs) of the flexible structure have been computed and compared to their rigid-body equivalents. These results show that the motions of the flexible structure are slightly larger over the range of the wave spectrum, which highlights the need to account for the deformations of the structure in the design process. A preliminary fatigue analysis in the frequency domain has been carried out and has showed the need to reinforce the tower if it is to withstand the combined wind and wave loads offshore. From the designer's perspective, we have demonstrated that the coupling between the different degrees of freedom due to the aerodynamic and restoring effects can be effectively accounted for as boundary conditions and do not require extensive time-domain simulations.

In the future, a lighter and therefore more economical design should also feature a shorter tower (part of which should be merged with the transition piece) as well as lighter, tapered braces. Once a robust design has been selected, a more thorough time-domain simulation of the whole structure including a detailed model of the blades, the rotor and the control system will of course be needed to capture non-linear and transient dynamic effects. Eventually, the combination of these advanced simulation tools with full-scale model testing should enable the construction of utility-scale floating wind farms capable of producing clean and renewable energy at an affordable cost for society.

7 References

1. Luis G. Arboleda-Monsalva, David G. Zapata-Medina, J. Dario Aristizabal-Ochoa
    Timoshenko beam-column with generalized end conditions on elastic foundation: Dynamic-stiffness matrix and load vector
    Journal of Sound and Vibration 310 (2008) 1057-1079

2. Igor A. Karnovsky, Olga I. Lebed
    Formulas for Structural Dynamics: tables, graphs and solutions
    New York: McGraw-Hill (2001)

3. J.R. Hutchinson
    Shear Coefficients for Timoshenko Beam Theory
    Journal of Applied Mechanics, 68, pp. 87-92

4. Eduardo Kausel
    Advanced Structural Dynamics
    Lectures Notes, MIT (2009)

5. Paul D. Sclavounos
    Ocean Wave Interactions with Ships and Offshore Energy Systems
    Lecture Notes, MIT (2011)

6. Kwang Hyun Lee
    Responses of Floating Wind Turbines to Wind and Wave Excitation
    Master's Thesis, MIT (2005)

7. Sungho Lee
    Dynamic Response Analysis of Spar Buoy Floating Wind Turbine Systems
    Master's Thesis, MIT (2008)

8. Denis Matha et al.
    Model Development and Loads Analysis of an Offshore Wind Turbine on a Tension Leg Platform, with a comparison to Other Floating Turbine Concepts
    NREL Subcontract Report SR-500-45891 (February 2010)

9. Jason M. Jonkman
    Dynamics Modeling and Loads Analysis of an Offshore Floating Wind Turbine
    Ph.D. Thesis, NREL (November 2007)

10. Herman Frederik Veldkamp
    Chances in Wind Energy – A Probabilistic Approach to Wind Turbine Fatigue Design
    Ph.D. Thesis, Technische Universiteit Delft (October 2006)

11. F.G. Nielsen, T.D. Hanson, B. Skaare
    Integrated Dynamic Analysis of Floating Offshore Wind Turbines
    Bergen, Norway: Hydro Oil and Energy (2007)

12. Dominique Rodier, Christian Cermelli, Alexia Aubault and Alla Weinstein
    WindFloat: A floating foundation for offshore wind turbines
    Journal of Renewable and Sustainable Energy 2, 033104 (2010)

13. Christian Lalanne
    Mechanical Vibration and Shock Analysis - Fatigue Damage (volume 4 – 2nd edition)
    Wiley, 2009

14. International Electrotechnical Commission (IEC)
    IEC 61400-3 Norm for Offshore Wind Turbines

15. European Committee for Standardisation (CEN)
    Eurocode 3: Design of steel structures, Part 1.9: Fatigue (2003)

16. Det Norske Veritas (DNV)
    Fatigue design of offshore steel structures
    DNV-RP-C203 (April 2010)

17. Det Norske Veritas (DNV)
    Position Mooring
    DNV-OS-E301 (June 2010)

18. International Institute of Welding
    Recommendations forFatigue Design of Welded Joints and Components
    IIW-1823-07 (December 2008)

19. K. Johannessen, T. S. Meling and S. Haver
    Joint Distribution for wind and wave in the Northern North Sea
    ISOPE, Stavanger, Norway (2001)

20. European Wind Energy Association (EWEA)
    2010 European Statistics (February 2011, available online)

21. Global Wind Energy Council (GWEC)
    Annual Market Update 2010 (2nd edition April 2011, available online)

22. European Environment Agency (EEA)
    Europe's Onshore and Offshore Wind Energy Potential (2009, available online)